CHAPTER

13

Biophysics of Voltage-Gated Ion Channels

Diane Lipscombe and Cecilia P. Toro

Voltage-gated ion channels (VGICs) are critical for rapid electrical signaling between and within cells, and sometimes across long distances. VGICs are the principal proteins that define cell excitability; neurons, muscles, and secretory cells use VGICs to generate regenerative responses—action potentials—that initiate major cellular events including synaptic vesicle exocytosis and muscle contraction. Homologs of VGICs are also found in choanoflagellates, which are microscopic, heterotrophic, single-celled and colony-forming eukaryotes. Thus, the appearance of VGIC-like proteins preceded the evolution of multicellular organisms and nervous systems, consistent with VGIC involvement in a range of cellular functions that are independent of their role in generating action potential-like signals.

PRINCIPAL FEATURES

The majority of VGICs convert changes in the membrane voltage, that may be as small as 1 mV or up to 100 mV during an action potential, into the rapid, efficient, and selective flow of one of three major cations across cell membranes: Na^+, K^+, and Ca^{2+}. Signature features of VGICs relative to other ion channels include:

- sensing small changes in the membrane voltage
- converting changes in membrane voltage into the rapid gating of an ion pore
- selecting for and supporting rapid flow of Na^+, Ca^{2+}, or K^+ ions across the cell membrane.

Highly precise biophysical methods are available to monitor each of these signature properties of VGICs—in real time and with remarkable resolution—offering unique insights into this essential family of proteins.

MAJOR FAMILIES OF VOLTAGE-GATED ION CHANNELS

Three major families of VGICs are expressed in the animal kingdom and they are most readily distinguished by the cation that they pass: sodium (Na_V), potassium (K_V), or calcium (Ca_V). The major classes of Ca_V channels are listed in Table 13.1. The different subtypes of Na_V and K_V channels are discussed elsewhere (e.g., Chapters 6, 12 and 14). All mammalian neurons studied to date express several different subtypes of each major family of VGIC to regulate several different cellular functions. This fact poses a significant challenge to study the biophysical properties of each type of VGIC in isolation from all others. Several neurotoxins, drugs, ions, and experimental approaches are used to separate the contributions of individual VGICs, define their individual biophysical characteristics, and determine their unique biological roles:

- Neurotoxins can be used to selectively inhibit specific families of VGICs. For example, puffer fish-derived tetrodotoxin selectively inhibits certain Na_V channels. Examples of natural toxins and venoms that act on VGICs are listed in Table 13.2.
- Drugs and other molecules can be used to selectively inhibit specific families of VGICs. For example, certain dihydropyridines are selective inhibitors of Ca_V1 channels.
- Various ions and salts can be used to inhibit certain VGICs. For example, barium (Ba^{2+}) and tetraethylammonium (TEA) inhibit several types of K_V ion channels.
- Ion substitution can eliminate currents through VGICs particularly if they have high selectivity to one particular ion species. For example, replacing Na^+ with the relatively impermeable cation choline eliminates currents through Na_V channels.

From Molecules to Networks.
DOI: http://dx.doi.org/10.1016/B978-0-12-397179-1.00013-0

TABLE 13.1 Ten major Ca_V channels are expressed in mammals; these are encoded by genes *CACNA1A* through *CACNA1I*, and *CACNA1S*. The tissue-specific and cell-specific expression patterns of each gene are unique. With the exception of *CACNA1S*, which is only expressed in skeletal muscle, all other *CACNA1* genes are expressed in the nervous system. $Ca_V2.1$ and $Ca_V2.2$ channels are the dominant presynaptic channels in mammalian nervous systems (Catterall, 2011), although $Ca_V1.3$ are in inner hair cells (Johnson and Marcotti, 2008) and $Ca_V1.4$ in photoreceptors (Bech-Hansen et al., 1998; Morgans, 2001). Ca_V1 (mainly $Ca_V1.2$) (Wheeler et al., 2012) and $Ca_V2.3$ (Parajuli et al., 2012) channels regulate calcium entry in postsynaptic dendrites. Postsynaptic $Ca_V1.3$ channels can mediate pacemaking (Putzier et al., 2009) and are implicated in the calcium-dependent death of dopaminergic neurons (Kang et al., 2012). In mouse, *CACNA1S* and *CACNA1C* gene knockouts are embryonic lethal and *CACNA1A* gene knockouts die shortly after birth. Several rare human hereditary mutations have been mapped to *CACNA1* genes; some are shown.

		Genes				
Channel	**Ion Current Types**	**Human**	**Human Disease[a]**	**Mouse, Rat**	***Drosophila***	***C. elegans***
$Ca_V1.1$	L	*CACNA1S* *1q32.1*	*Hypokalemic periodic paralysis, type 1*	*Cacna1s*	*Ca-α1D*	*egl-19*
$Ca_V1.2$	L	*CACNA1C* *12p13.33*	*Brugada syndrome 3* *Timothy syndrome*	*Cacna1c*		
$Ca_V1.3$	L	*CACNA1D* *3p21.1*	*Sinoatrial node dysfunction and deafness*	*Cacna1d*		
$Ca_V1.4$	L	*CACNA1F* *Xp11.23*	*Aland Island eye disease* *Cone-rod dystropy, X-linked, 3* *Night blindness, congenital stationary (incomplete), 2A, X-linked*	*Cacna1f*		
$Ca_V2.1$	P/Q	*CACNA1A* *19p13.2*	*Episodic ataxia, type 2* *Migraine, familial hemiplegic, 1* *Migraine, familial hemiplegic, 1, with progressive cerebellar ataxia* *Spinocerebellar ataxia 6*[#]	*Cacna1a*	*cac*	*unc-2*
$Ca_V2.2$	N	*CACNA1B* *9q34.3*		*Cacna1b*		
$Ca_V2.3$	R	*CACNA1E* *1q25.3*		*Cacna1e*		
$Ca_V3.1$	T	*CACNA1G* *17q21.33*		*Cacna1g*	*Ca-α1T*	*cca-1*
$Ca_V3.2$	T	*CACNA1H* *16q13.3*		*Cacna1h*		
$Ca_V3.3$	T	*CACNA1I* *22q13.1*		*Cacna1i*		

[a]*New mutations are identified on an ongoing basis, so the reader is referred to various open source sites such as The HUGO Gene Nomenclature Committee, a curated online repository of HGNC-approved gene nomenclature and associated resources (genenames.org) and Online Mendelian Inheritance in Man, a compendium of human genes and genetic phenotypes (OMIM®, omim.org). Disorders linked to* CACNA1 *genes do not necessarily arise because of alterations in channel biophysical properties. For example, there is evidence for internal ribosomal entry sites in* CACNA1A *that express a transcription factor implicated in spinal cerebellar ataxia 6 (Du et al., 2013). By contrast to mammalian genomes,* Drosophila *and* C. elegans *genomes only contain three Ca_V genes, one encoding each of the major subtypes; see Lipscombe et al. (2013).*

- Cell-attached patch clamp recordings can isolate the activity of specific VGICs that are found at relatively high density in specialized regions of neuronal membranes, such as Na_V channels at axonal nodes of Ranvier and Ca_V channels at presynaptic nerve terminals.
- cDNA cloning and heterologous expression of individual VGIC subunits are used to generate cells enriched in one specific class of VGIC. For example, many VGICs express well in *Xenopus* oocytes and human embryonic cell lines that have low endogenous levels of VGICs.

Each major family of VGIC has highly, although not perfectly, discriminating ion pores whose ion selectivity is determined by the unique, conserved amino acid sequence motifs that line the narrow part of their selectivity filters within their respective pore domains (S5-S6; Fig. 13.1A). High selectivity for a single ion is a feature that is common among VGICs of the same family. By contrast, ion channel gating characteristics within and across the major VGICs families can vary substantially. Ion channel gating is also strongly influenced by many signaling molecules including Ca^{2+}, cyclic nucleotides, kinases, phosphates, calcium/calmodulin, $\beta\gamma$ dimers of

TABLE 13.2 Neurotoxins That Inhibit Voltage-Gated Ion Channels. Voltage-gated ion channels are targeted by a wide variety of plant and animal species that produce neurotoxins. Here we describe some of the best-studied neurotoxins. Neurotoxins can selectively bind one specific isoform of VGIC (e.g., ω-conotoxin GVIA binds and inhibits $Ca_V2.2$) or they can bind to several closely related members of channels (e.g., ciguatoxin binds to site 5 of Na_Vs). Neurotoxins are used by predatory animals (e.g., calciseptine is produced by the black mamba snake) as well as animals and plants that are prey (e.g., batrachotoxin-producing poison-dart frogs and acotine-producing heather plants). Depending on their target channel(s), neurotoxins act as agonists or antagonists. For example, many neurotoxins act as antagonists on K_V channels, and others act as agonists on Na_V channels; both mechanisms result in overexcitation of the target neuron. Several types of animals are particularly prolific in their production of diverse neurotoxins; these include sea anemones (Castaneda and Harvey, 2009), cone snails (Knapp et al., 2012), and spiders (Pringos et al., 2011).

Neurotoxin	Target	Effect	Source
VOLTAGE-GATED CALCIUM CHANNEL TOXINS			
ω-Agatoxin IVA,B	$Ca_V2.1$	Antagonist: stabilizes closed state	American funnel web spider *Agelenopsis aperta*
Calcicludine	Ca_V1s	Antagonist	Green mamba snake *Dendroaspis angusticeps*
Calciseptine	$Ca_V1.2$	Antagonist	Black mamba snake *Dendroaspis polylepsis polylepsis*
ω-Conotoxin GVIA, MVIIA, SVIB	$Ca_V2.2$	Antagonist: pore blocker	Cone snails *Conus geographus, magus*, and *striatus*
ω-Conotoxin MVIIC	$Ca_V2.1$	Antagonist: pore blocker	Cone snail *Conus magus*
Glycerotoxin	$Ca_V2.2$	Agonist: causes a hyperpolarizing shift in voltage-dependence of activation	Marine blood worm *Glycera convoluta*
ω-Grammotoxin SIA	Ca_V2s	Antagonist: slows activation and causes a depolarizing shift in voltage-dependence of activation	Tarantula *Grammostola spatulata*
Kurtoxin	Ca_V1 $Ca_V2.2$ Ca_V3	Antagonist: slows activation, accelerates deactivation	Scorpion *Parabuthus transvaalicus*
Kurtoxin	$Ca_V2.1$	Agonist: slows deactivation	Scorpion *Parabuthus transvaalicus*
ω-Phonetoxin IIA	Ca_V2s	Antagonist	Armed spider *Phoneurtria nigriventer*
SNX-325	$Ca_V2.2$	Antagonist	Tube web spider *Segestria florentina*
SNX-482	$Ca_V2.3$	Antagonist	African tarantula *Hysterocrates gigas*
Tx3-4	$Ca_V2.1$	Antagonist	Armed spider *Phoneurtria nigriventer*
VOLTAGE-GATED POTASSIUM CHANNEL TOXINS			
BgK	K_V1s	Antagonist	Sea anemone *Bunodosoma granulifera*
Charybdotoxin (α-KTx2.1)	$K_V1.3$ $K_V1.2$	Antagonist: pore-blocker	Scorpion *Leiurus quinquestriatus*
Dendrotoxin	K_Vs	Antagonist	Eastern green mamba snake *Dendroaspis angusticeps*
Hanatoxin	$K_V2.1$	Antagonist: causes a depolarizing shift in the voltage-dependence of activation; speeds deactivation	Tarantula *Grammostola spatulata*
HsTx1	$K_V1.1$ $K_V1.3$	Antagonist	Scorpion *Heterometrus spinnifer*
Maurotoxin	$K_V1.2$	Antagonist: pore-blocker	Tunisian chactoid scorpion *Scorpio maurus*
ShK	$K_V1.3$, $K_V3.2$	Antagonist	Sea anemone *Stichodactyla helianthus*
VOLTAGE-GATED SODIUM CHANNEL TOXINS			
Aconitine	Na_V	Alters ion selectivity	Aconitum plant (aka queen of poisons or monkshood)
Aconitine	Na_V (site 2)	Agonist: causes a hyperpolarizing shift in voltage-dependence of activation; slows or abolishes inactivation; reduces single-channel conductance	

(*Continued*)

TABLE 13.2 (Continued)

Neurotoxin	Target	Effect	Source
δ-Atracotoxins	Na_V (site 3)	Agonist: slows inactivation	Sydney funnel-web spider *Atrax robutus*
Batrachotoxin	Na_V (site 2)	Agonist: causes a hyperpolarizing shift in voltage-dependence of activation; slows or abolishes inactivation; reduces single-channel conductance	Colombian poison dart frogs *Phyllobates aurotaenia*
Brevetoxin	Na_V (site 5)	Agonist: causes a hyperpolarizing shift in voltage-dependence of activation; slows or abolishes inactivation	Dinoflagellates
Ciguatoxin	Na_V (site 5)	Agonist: causes a hyperpolarizing shift in voltage-dependence of activation; can left-shift steady-state inactivation and increases rate of recovery from inactivation	Dinoflagellates
δ-conotoxins	Na_V (site 6)	Agonists: cause a hyperpolarizing shift in voltage-dependence of activation; slow inactivation	Multiple cone snails
μ-conotoxins	Na_V1 (site 1)	Antagonists: pore-blockers	Multiple cone snails
Coral Toxin	Na_V	Agonist: slows inactivation	Coral *Goniopora*
Grayanotoxins	Na_V (site 2)	Agonist: causes a hyperpolarizing shift in voltage-dependence of activation; slows or abolishes inactivation; reduces single-channel conductance	Heather plants
Phonetoxin 2-6	Na_V	Agonist: slows inactivation	Armed spider *Phoneurtria nigriventer*
Pompilidotoxins	Na_V	Agonists: slow inactivation	Solitary wasps *Anoplius samariensis* and *Batozonellus maculifrons*
ProTx-I and II	Na_V1s	Antagonists: cause a depolarizing shift in the voltage-dependence of activation	Tarantula *Thrixopelma pruriens*
Saxitoxin	Na_V (site 1)	Antagonist: blocked Na conductance	Dinoflagellates
Scorpion α-toxins	Na_V (site 3)	Agonists: slow inactivation	Scorpions
Scorpion β-toxins	Na_V	Agonists: cause a hyperpolarizing shift in voltage-dependence of activation	Scorpions
Sea anemone toxins	Na_V (site 3)	Slowed inactivation	Sea anemones
Tetrodotoxin	Na_V (site 1)	Blocked Na conductance	Pufferfish, Rough-skinned newt, blue-ringed octopus and others via *Vibrio* bacteria consumption
Veratridine	Na_V (site 2)	Hyperpolarizing shift in voltage-dependence of activation; slowed or abolished inactivation; reduction in single-channel conductance	Lilaceous plants

G proteins, and association with other proteins. These molecules tend to act by stabilizing different conformational states of the ion channel. For example, they might increase the likelihood that the channel will spend more time open or in one of several closed or inactivated states. Signaling molecules can modulate the biophysical properties of VGICs via G protein coupled receptors; this is the mechanism of action of most neurotransmitters, neurohormones, and many drugs that regulate neuronal excitability and synaptic efficacy.

VGICS ARE HIGHLY SENSITIVE TO MEMBRANE VOLTAGE BUT CURRENT FLOW THROUGH ALL ION CHANNELS IS INFLUENCED BY VOLTAGE

The S4 α-helices of VGICs are amphipathic and traverse the membrane electrical field. Ion channel activation is initiated by the outward movement of the S4 α-helices with respect to the rest of the ion channel protein in response to membrane depolarization. The

translocation of S4 α-helices is required for the central-axis ion pore to open (Fig. 13.1A, pore domain). The precise and efficient coupling between membrane depolarization and ion channel opening is unique to VGICs, but membrane voltage influences ion flow through *all* ion channels:

- Ions are charged molecules. Therefore, the rate at which they move through the open pore is strongly dependent on voltage, and more specifically on the driving force.
- Ion channels span the membrane electric field which can be quite substantial, $\sim 10^7$ V/m. Consequently, the gating of all ion channels is influenced to some degree by the membrane voltage.

Additionally, the unique features of certain ion channels enhance their sensitivity to voltage:

- Certain chloride ion channels (CLC) are gated by voltage, although with an order of magnitude lower sensitivity compared to VGICs described here.
- Ion flow through several ion channels, including NMDA receptor ion channels and inwardly rectifying K^+ channels, is strongly dependent on membrane voltage. For example, Mg^{2+} and polyamines inhibit the flow of cations through these ion channels by occluding the ion channel pore. The inhibitory actions of Mg^{2+} and polyamines are strongly influenced by membrane voltage.
- Gating of connexin channels (Chapter 9) at gap junctions that span the plasma membranes of two cells is strongly affected by the trans-junctional voltage (V*j*) across cells.
- Voltage-gated proton channels, like VGICs, are highly selective for the ion that they conduct (H^+), but these channels are structurally distinct from VGICs and they lack a VGIC-like pore domain.

This chapter focuses on canonical, tetrameric VGICs; each has exquisite sensitivity to voltage and a selective cation pore (see Fig. 13.1A).

ABNORMAL BIOPHYSICAL PROPERTIES OF VGICS AND HUMAN DISEASE

Biophysical analyses of VGIC proteins with disease-causing mutations have given insight into disease mechanisms and have led to important discoveries related to ion channel structure and function. In the following examples, single point exonic mutations in human genes encoding Ca_V and Na_V channels were identified in patients with rare hereditary disorders (see Fig. 13.1B for position of the mutations on the VGIC transmembrane structure).

Normokalemic Periodic Paralysis

The rare autosomal dominant hereditary disorder normokalemic periodic paralysis (NormoPP) is present in 1 of every 100,000 people. Mutations in one of two VGIC genes, *CACNA1A* and *SCN4A* that encode $Ca_V1.1$ and $Na_V1.4$ channels of skeletal muscle respectively, are often involved in this disorder. NormoPP is characterized by recurrent episodes of severe muscle weakness that can last for hours to days. Typically, one of two outermost arginines (R; basic amino acid) located in the voltage-sensing S4 α-helices of either $Ca_V1.1$ or $Na_V1.4$ channels are mutated (Fig. 13.1A). Despite their localization to S4 α-helices, the effects of NormoPP mutations on channel gating were not consistent or sufficiently different from wild-type channels to account for the disease. The similarity between Na^+ currents recorded from *Xenopus* oocytes expressing wild-type and R669G mutant $Na_V1.4$ channels is illustrated in Figs. 13.2A1 and 13.2A2 (Sokolov et al., 2008).

By biophysical analyses, Catterall and colleagues revealed that mutations of the outermost arginines in S4 of Na_V channels resulted in the creation of an anomalous gating pore current that is not present in normal muscle. This gating pore current is distinct from the main ionic current that is generated by ions flowing through the central ion pore domain (Fig. 13.2; ionic Na_V currents are shown in the upper panels (A1, A2) and gating pore currents in the middle panels (B1, B2)). Cations are thought to leak through the mutant gating pore when Na_V channels are in the resting state thereby leading to muscle membrane depolarization and Na^+ overload. Thus, biophysical analyses were used to determine the molecular basis of NormoPP (Sokolov et al., 2007; Sokolov et al., 2008). *Xenopus* oocytes expressing wild-type and mutant $Na_V1.4$ channel currents are illustrated in Fig. 13.2. Gating pore currents were isolated and measured after inhibiting the central ion pore using tetrodotoxin (Fig. 13.2B1, 13.2B2; see also Table 13.2). When the central ion pore is inhibited, the expected linear leak current is measured in cells expressing wild-type $Na_V1.4$ channels (Fig. 13.2B1, 13.2C1), but there is an additional unexpected gating pore current observed as the membrane potential is depolarized in cells expressing the $Na_V1.4$ R669G channel mutant (Fig. 13.2B2, 13.2C2). This is a gain-of-function mutation because the gating pore current is not a normal feature of $Na_V1.4$ channels.

Erythromelalgia and Paroxysmal Extreme Pain Disorder (PEPD)

Erythromelalgia and paroxysmal extreme pain disorder (PEPD) are two diseases associated with abnormal episodic pain. The *SCN9A* gene is mutated

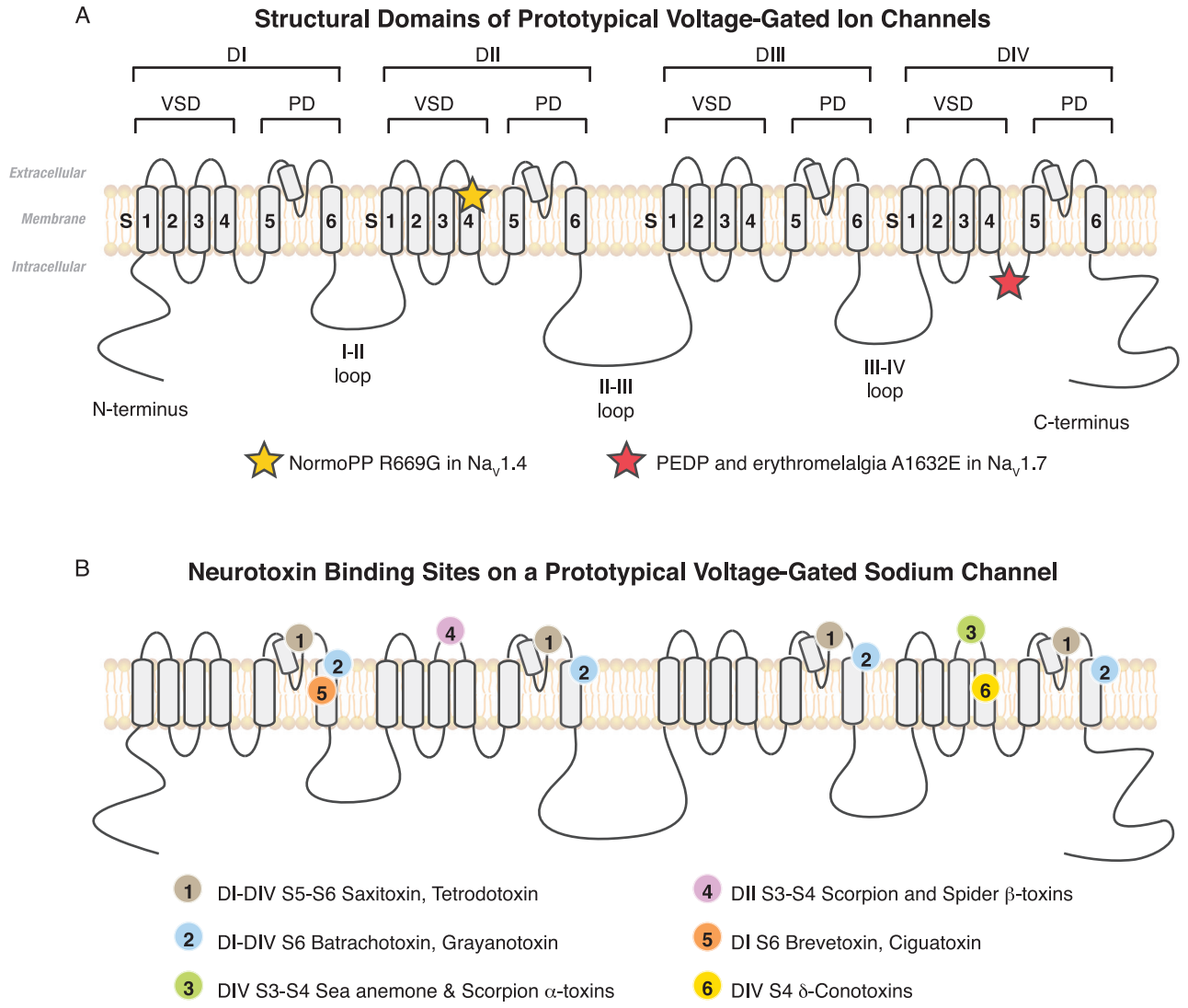

FIGURE 13.1 Transmembrane topology of Na$_V$ and Ca$_V$ voltage-gated ion channels. Transmembrane, intracellular, and extracellular regions of α_1-subunits of voltage-gated ion channels are illustrated. **A**, α_1-subunits formed by four domains (DI, DII, DIII, DIV); each contain six transmembrane spanning α-helices (S1–S6), for a total of 24 complete crossings of the membrane. α_1-subunits of Na$_V$ and Ca$_V$ channels are single proteins encoded by single genes, whereas K$_V$ channels are formed by the association of four separate proteins that each correspond to one domain (S1–S6). The four proteins that associate to form a functional K$_V$ channel can all be encoded by the same gene (homotetrameric) or by different genes (heterotetrameric). S1–S4 is the voltage-sensor domain (VSD), and each VSD contains an amphipathic S4 α-helix that contains basic amino acids (arginines or lysines) every third or fourth amino acid around the α-helical turns. The VSD forms the gating pore that forms the track for S4 to move outward during gating (see Fig. 13.4). S5–S6 of each domain is called the pore domain (PD); the four PDs from DI–DIV associate symmetrically to create the central axis ion pore. Each PD contains a short pore α-helix. The intracellular loops that connect the major domains are labeled. Locations of the normokalemic periodic paralysis (NormoPP) mutation R669G in Na$_V$1.4 channels (Sokolov et al., 2008; also see Fig. 13.2) and the PEDP/erythromelalgia mutation A1632E in Na$_V$1.7 channels (Estacion et al., 2008; also see Fig. 13.3) are shown. **B**, Major binding sites of various neurotoxins which act on Na$_V$ channels (neurotoxins are listed in Table 13.2).

in ~15% of individuals with inherited erythromelalgia, in ~66% of families with autosomal dominant inherited PEPD, and in some families with symptoms of both disorders (Fertleman et al., 2006; Dib-Hajj et al., 2005; Estacion et al., 2008). The *SCN9A* gene encodes Na$_V$1.7 channels that are expressed in primary sensory neurons of dorsal root ganglia and sympathetic ganglia. Biophysical analyses of Na$_V$1.7 channels with disease-causing mutations reveal gain-of-function properties that are consistent with disease symptoms. For example, a mutation in the *SCN9A* gene was identified in a family with symptoms characteristic of both erythromelalgia and PEPD (Estacion et al., 2008). The mutation A1632E (uncharged alanine

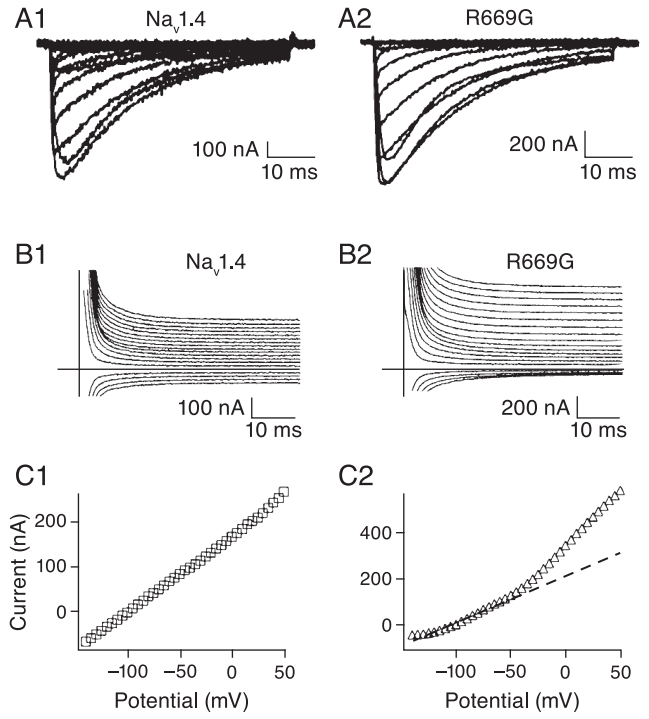

FIGURE 13.2 The normokalemic periodic paralysis (NormoPP) disease-causing mutation R669G creates an anomalous gating pore in $Na_V1.4$ channels. A1, A2, series of Na_V currents recorded from *Xenopus* oocytes transiently expressing either wild-type $Na_V1.4$ or R669G mutant channels. Currents were evoked by test depolarizations from −90 mV to +50 mV applied in 10 mV increments from a holding potential of −100 mV. Wild-type and mutant $Na_V1.4$ channel currents are similar. B1, B2, Gating pore currents were isolated after inhibiting the central ion pore with 1 μM tetrodotoxin (TTX). Gating pore currents are observed in cells expressing R669G mutant channels (B2, right) whereas only leak currents are measured in cells expressing wild-type $Na_V1.4$ channels (B1, left). Currents shown were evoked by voltage steps from −140 to +50 mV applied in 5 mV increments from a holding potential of −100 mV (every second trace is shown). C1, C2, Amplitude of currents recorded in the presence of TTX plotted against test potential. The dashed lines represent background linear leak in representative cells and the additional current recorded in cells expressing R669G at potentials positive to ~ −40 mV is the gating pore current. *Adapted from reference Sokolov et al. (2008) with permission from the National Academy of Sciences, U.S.A. Copyright 2008 National Academy of Sciences, U.S.A.*

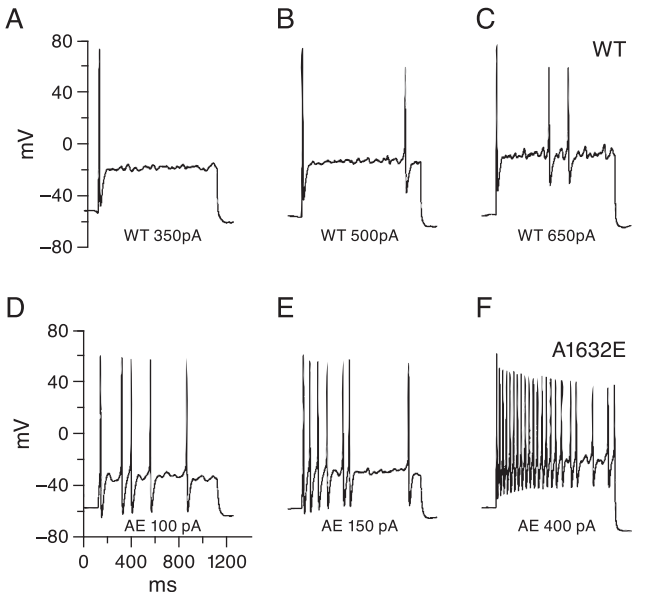

FIGURE 13.3 Current-clamp recordings from dorsal root ganglia neurons transfected with wild-type or A1632E $Na_V1.7$ channels. A−F, Responses of a current-clamped DRG neuron overexpressing wild-type (A−C) or A1632E (D−F) $Na_V1.7$ channels to a series of suprathreshold depolarizing current stimuli of the size indicated below each recording. The threshold for action potential firing is lower, and the number of action potentials evoked is higher in DRG neurons expressing A1632E mutant $Na_V1.7$ channels compared to those expressing wild-type $Na_V1.7$ channels. *Adapted from Estacion et al. (2008) with permission from the Society for Neuroscience.*

to acidic glutamate) in the DIVS4-DIVS5 region of $Na_V1.7$ (see Fig. 13.1A for location of the mutation) alters several biophysical properties of the channel. Mutant $Na_V1.7$ channels are more likely to open at hyperpolarized voltages and less likely to inactivate compared to wild-type $Na_V1.7$ channels. The impact of a disease-causing mutation in $Na_V1.7$ on neuronal excitability is illustrated (Fig. 13.3). $Na_V1.7$ A1632E channels expressed in small dorsal root ganglia neurons result in hyperexcitability; neurons expressing $Na_V1.7$ A1632E fire more readily and at higher frequencies (Fig. 13.3D, 13.3E, 13.3F) compared to neurons expressing wild-type $Na_V1.7$ channels (Fig. 13.3A, 13.3B, 13.3C) (Estacion et al., 2008). This is also a gain-of-function mutation because $Na_V1.7$ channels, and neurons that express them, exhibit properties not normally observed.

Autosomal Dominant Lateral Temporal Lobe Epilepsy with Auditory Features

Autosomal dominant lateral temporal lobe epilepsy with auditory features (ADPEAF) is a rare epilepsy associated with auditory symptoms that include buzzing, humming, or ringing. 50% of ADPEAF patients have mutations in the leucine-rich glioma inactivated gene 1 (*LGI1*). Biophysical studies have shown that the Lgi1 protein, which is in a complex with presynaptic $K_V1.1$ and $K_V\beta1$ subunits, prevents rapid inactivation of $K_V1.1$ currents. Disease-causing mutations in the Lgi1 protein render it unable to prevent fast inactivation of presynaptic $K_V1.1$ currents. Faster than normal inactivation of presynaptic $K_V1.1$ currents, resulting from the lack of effect of Lgi1, is thought to result in a gain-of-function phenotype which is hypothesized to result in increased synaptic activity that could trigger epileptic activity (Schulte et al., 2006).

STRUCTURAL FEATURES ASSOCIATED WITH UNIQUE BIOPHYSICAL PROPERTIES OF VGICS

VGICs have a tetrameric structure formed by symmetrical association of four structurally homologous domains that create a central-axis ion pore. Each one of the four main domains of VGICs is comprised of four transmembrane-spanning α-helices (S1–S4) that form the voltage-sensing domain (VSD), and two additional transmembrane-spanning α-helices, S5 and S6, that are linked by a loop that contains a short α-helix and that lines the ion pore (Fig. 13.1A). The amount of time VGICs spend in discrete conformations, closed, open, and inactivated and the rate of transition between them during activation, deactivation, and inactivation are influenced by several structural elements (Fig. 13.1A):

- The S4 α-helices of VSDs are critical for sensing the transmembrane voltage and initiating activation and deactivation.
- The S4–S5 linkers couple the VSDs to the Pore Domain (PD).
- Amino acids in the pore lining segments of S5–S6 in the PD are essential for ion selectivity and permeation when the ion channel is open.
- Intracellular regions including the N-terminus, C-terminus, III-IV linker, and others influence inactivation.

Voltage-Sensing Domains

The VSDs are formed by transmembrane-spanning α-helices S1–S4. S4 is located in the center of a vestibule that is created by the surrounding S1–S3 helices. S4 is amphipathic; it contains a high density of basic amino acids: usually an arginine every third or fourth amino acid around the α-helical turn. As discussed above, a gating pore is formed within each VSD within which S4 moves with respect to surrounding S1–S3 helices. The outward movement of S4 during depolarization displaces charge (carried by basic amino acids) and is the origin of the "ON" gating current that precedes the ionic current (see Fig. 13.4). The outward displacement of gating charge during activation is followed by the return inward displacement of "OFF" gating charge during deactivation (Fig. 13.4). Ions do not normally transit the gating pore, but as discussed above, disease-causing mutations of outer arginines in S4 can create an anomalous ion pore and ion leak (Fig. 13.2).

S4 α-Helices of Voltage Sensing Domains (VSDs)

The gating current is the first biophysical event in the sequence of conformational changes that occur during VGIC activation (Armstrong and Bezanilla, 1974). An estimated 13 electronic charges are displaced in K_V *shaker* channels during activation (Schoppa et al., 1992). This at first seems unlikely because it suggests the S4 helices would have to move substantially, from one side of the membrane to the other, to displace that number of charges. However, the electric field does not traverse the width of the lipid bilayer but rather it is highly focused around each S4 helix within the gating pore vestibule (Starace and Bezanilla, 2004; Ahern and Horn, 2005). Therefore, the S4 helices only need to move relatively short distances to accomplish the electronic charge displacement measured during gating (Bezanilla, 2008) (Fig. 13.4).

The S4 helices within domains DI, DII, and DIII of Na_V channels are closely linked to the rapid movement of gating charge and to pore opening. There is evidence of cooperativity among S4 helices, such that the displacement of one S4 increases the likelihood that the others will move. However, the Hodgkin and Huxley model of Na_V channel gating assumed Na_V channel opening required the movement of three activation gates that moved independent of the other (see Fig. 13.9 and Chapter 14). Additionally, the S4 in DIV of Na_V channels might participate in inactivation (Bezanilla, 2008).

Gating currents and ionic currents measured in cells expressing high levels of $Ca_V2.2$ channels in a mammalian cell line are illustrated in Fig. 13.4 (see Table 13.1 for an explanation of Ca_V channel nomenclature). Two different methods were used to isolate the smaller, transient gating currents from larger, more sustained ionic currents. The panels on the left show both gating and central pore ionic Ca_V currents measured in the same cell in response to depolarizing voltage steps (test pulses). Transient outward gating currents develop immediately following the voltage steps, as the membrane is depolarized to about −40 mV. But, at more depolarized voltages, early gating currents are obscured by subsequent, larger inward ionic currents (Fig. 13.4; left). "ON" gating currents are measured in isolation from ionic currents at the ionic reversal potential (also called E_{Rev}); this is the voltage at which there is no net flow of ionic current. In the example in Fig. 13.4, a three-step protocol is used: a negative prepulse that removes inactivation and returns all Ca_V channels to the available, closed state (also see Fig. 13.9 for kinetic model); test pulses of increasing magnitudes; and a final step to the ionic reversal potential to measure the remaining "ON" gating current. The total gating charge that develops at maximum activation is equal to the sum of the "ON" gating charge during the test pulse and the "OFF" gating charge at the ionic reversal potential.

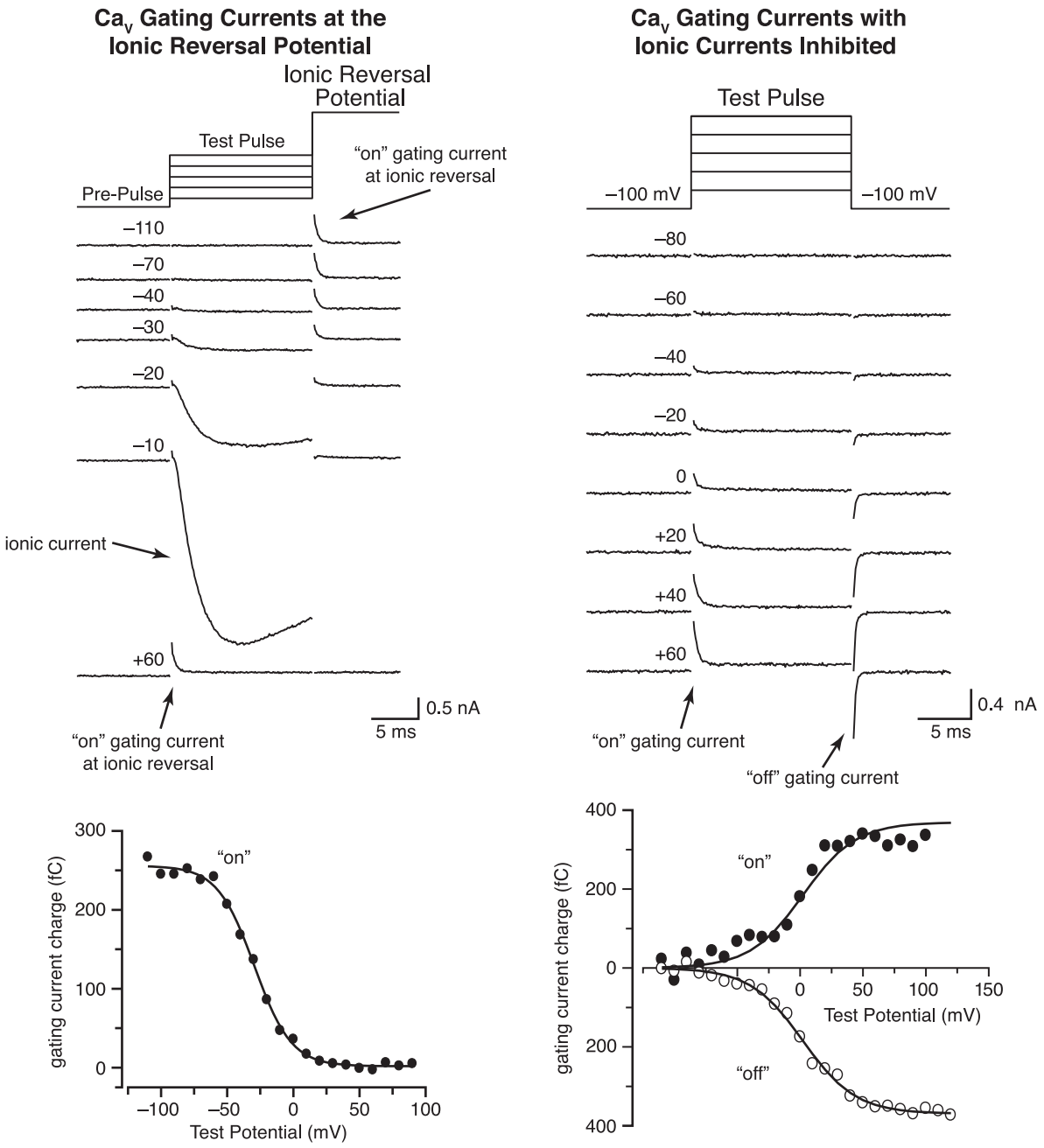

FIGURE 13.4 Comparison of $Ca_V2.2$ gating currents measured by two methods: at the ionic reversal potential using barium as the charge carrier and with ionic currents blocked by a combination of cobalt and cadmium. Currents were recorded from a variant of the human embryonic kidney HEK293 cell line (tsA201) stably expressing $Ca_V2.2$ channels together with auxiliary subunits. Select current traces are shown. Left, step depolarizations of increasing size were applied from a holding potential of −120 mV in 10 mV increments before a final step to the ionic reversal potential, +60 mV. At the ionic reversal potential, gating currents are isolated ("on" gating current). Scale bars: 0.5 nA, 5 ms. The decrease in the "on" gating current measured at +60 mV is plotted as a function of the preceding test voltage and fit with a single Boltzmann function with parameters: $V_{1/2} = 29.4$ mV and $k = 13.9$ mV. Right, a series of current traces showing "on" and "off" gating currents recorded at the start and end of test depolarizations, in the presence of 2 mM cobalt and 0.2 mM cadmium that inhibit ionic current. Gating currents were activated by test depolarizations (− 100 mV to +100 mV) as indicated from a holding potential of −120 mV. Scale bars: 0.4 nA, 5 ms. The total outward gating charge moved during the "on" gating current is the same as the total inward gating charge moved during the "off" gating current. Single Boltzmann function fit to the data had values $V_{1/2} = -1.7$ mV and $k = 12.5$ mV. Cadmium and cobalt shift the gating current activation curve to voltages ~30 mV more depolarized compared to those recorded at the ionic reversal potential in the presence of 2 mM barium (left). *Adapted from Lin et al. (2004).*

In Fig. 13.4, the voltage dependence of gating charge (Q_{on}, measured in fCoulombs) is plotted against the size of the test pulse. This type of protocol, which measures gating currents at the ionic reversal potential, allows for gating and ionic currents to be measured under identical recording conditions. In Fig. 13.4, in the panel on the right, only gating currents are measured in response to a series of depolarizing test pulses. In this experiment, ionic currents were inhibited by a combination of cobalt and cadmium to prevent the flow of Ca^{2+} or Ba^{2+} ions through the central ion pore. Transient outward "ON" gating currents develop immediately following the step as the S4 helices move outward, and transient inward "OFF" gating currents develop immediately after the step is turned off, and as the S4 helices return to their resting positions. In this experiment Q_{on} and Q_{off} are measured and compared. Q_{on} and Q_{off} are equal in magnitude as expected if they reflect the movement of charged particles or voltage sensors, outward during activation and inward during deactivation (as the channels close). However, when some ion channels inactivate, the voltage sensors are immobilized and their return to the closed position is slowed and not resolvable above the background signal. This results in an apparent loss of gating charge $Q_{off} < Q_{on}$. The voltage-dependence of the gating charge (Q-V) is well described by a Boltzmann function (see "Steady State Current Voltage Relationships" section and Chapter 14), consistent with the movement of multiple gating particles (voltage sensors) before ion channel opening (see Fig. 13.9).

The Linker between Voltage-Sensing Domain and Pore Domain

In VGICs the S4–S5 intracellular region links the VSD to the PD (Fig. 13.1A). The S4–S5 linker is thought to transmit the movement of the S4 α-helices within the VSDs to the gating of the ion pore (Long et al., 2005; Chen et al., 2001). The main central pore gate resides toward the cytoplasmic side of the channel and is formed by a twisted bundle of 8 α-helices or four pairs of S5–S6 from each domain (DI–DIV; Fig. 13.1A). When closed, this region in VGICs prevents the movement of ions through the pore, but during activation, the displacement of S4 is transmitted to the PD via S5–S6 and results in an iris-like opening of the gate, permitting ion flow. The S4–S5 linker may also be the site of action of the membrane phospholipid phosphatidylinositol-4,5-bisphosphate (PIP_2) (Rodriguez-Menchaca et al., 2012), a critical priming molecule required for several—although not all—VGICs to be available for opening (see below and Fig. 13.13).

The Pore Domain

The S5–S6 α-helices from each domain associate to form the pore domain (PD). The PD creates the lining of the ion pore, the narrow part of which selects the specific ion (K^+, Na^+, and Ca^{2+}), and the main gate toward the cytoplasmic side of the ion pore formed by the convergence of S5 and S6 α-helices. Highly conserved amino acids form the narrow selectivity filter for each major VGIC family, K_V, Na_V, and Ca_V, and these interact with the permeating ion and/or its hydration shell. The molecular basis of high K^+ selectivity and high ion flow rate was solved when the first 2-angstrom resolution crystal structure of a selective ion channel pore was determined (Doyle et al., 1998). These important experiments are described in detail elsewhere. The ion selectivity filters of Ca_V and Na_V channels are wider compared to K_V and, based on the crystal structure of the bacterial sodium channel NaChBac from *Bacillus halodurans*, Na^+ ions are partially hydrated as they move through the selectivity filter (Payandeh et al., 2011). The biophysics of Ca^{2+} ion selection and ion flow through Ca_V1 channels was studied extensively prior to knowledge of the crystal structure of any VGIC ion pore (Almers and McCleskey, 1984; Hess and Tsien, 1984; Friel and Tsien, 1989; Yang et al., 1993). An example of these insightful biophysical experiments is described in later section (Fig. 13.15).

REGIONS OF VGICS THAT REGULATE INACTIVATION

VGICs also inactivate. In the inactivated state, VGICs cannot conduct ions but, different from the closed state, membrane depolarization cannot open the channel (see Fig. 13.9). Recovery from inactivation requires a return of the membrane potential to a hyperpolarized value—for varying lengths of time that depend on the type of inactivation. For example, many VGICs exhibit at least two forms of inactivation, fast and slow, that are distinguished according to their kinetics. Different mechanisms and structural elements can be involved in fast inactivation and slow inactivation of VGICs. Returning the membrane voltage to negative values allows the S4 helices to return to their resting closed state so they are poised for subsequent activation and, in some channels, return of an inactivation particle to a position that permits ion flow (see Fig. 13.9). The time course and voltage-dependence of entry into inactivation, and similarly the recovery from inactivation, can vary substantially among different classes of VGICs, and can be influenced by many different factors including calcium/calmodulin, phosphorylation, and association with other proteins (see Fig. 13.17). Biophysical

analyses provide vital information about the mechanisms of VGIC inactivation. Several different regions of VGICs are known to affect inactivation including N-termini, C-termini, intracellular linkers, pore regions and transmembrane spanning α-helices. N-type (fast) and C-type (slow) inactivation are prominent and distinguishing features of different K_V channels. For example, N-type inactivation is relatively fast and involves the N-terminus of the VGIC plugging the intracellular region of the ion pore thereby preventing ion flow. By contrast, C-type inactivation is relatively slow and depends on protein interactions with the C-terminus of VGICs and immobilization of the S4 helices. Similarly, different Ca_V channels exhibit calmodulin-dependent inactivation and facilitation depending on the amino acid compositions of their C-termini and interactions with other proteins (Peterson et al., 1999; Lee et al., 1999; Lee et al., 2003; Yang et al., 2006; Leal et al., 2012).

BIOPHYSICAL PROPERTIES OF VOLTAGE-GATED ION CHANNELS AND NEURONAL FUNCTION

The unique biophysical features of VGICs offer critical insight into their functional roles in neurons. A wide range of time courses and voltage-dependencies of channel opening and closing, entry into and recovery from inactivation, and ion selectivity all define different classes of VGICs. A spectrum of biophysically distinct ion channels contribute to rapid changes in the membrane potential during action potential waveforms, link membrane depolarization to local and rapid increases in intracellular calcium, and act as voltage sensors independent of their ability to support ion permeation.

Action Potential Waveforms

The most studied role of VGICs is to support large, rapid and transient changes in the permeability of the membranes of excitable cells to Na^+, K^+ and Ca^{2+} to generate action potentials. As will be discussed in detail in Chapters 12 and 14, the rapid gating of Na_V channels dominates and underlies the upstroke of action potentials in most cells, while the slightly slower activation kinetics of a certain class of K_V channel coupled with rapid inactivation of Na_V channels dominates and underlies the falling phase—repolarization phase—of most action potentials in mammalian neurons. In some neurons and in muscle cells, Ca_V channels shape and trigger action potentials and regulate firing frequency (e.g., thalamic reticular neurons shown in Fig. 13.5). Ca_V channels, not Na_V channels, generate action potential-like waveforms in neurons of the nematode *C. elegans*, in muscles of crustaceans, and in certain other cells (Fatt and Ginsborg, 1958; Hagiwara and Byerly, 1981; Shtonda and Avery, 2005).

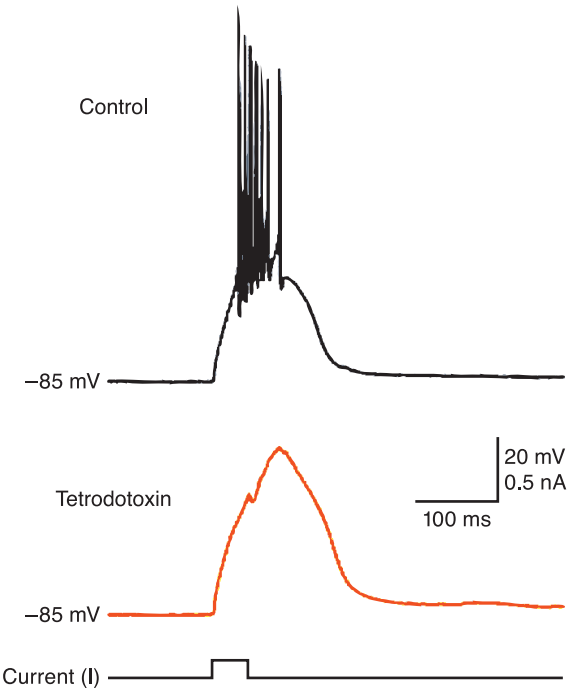

FIGURE 13.5 Fast Na_V action potentials and slow Ca_V depolarizations recorded from a GABAergic thalamic reticular nucleus neuron. A somatic recording showing that a depolarizing current step evokes a burst of fast action potentials riding on the top of a slower, longer lasting depolarization. Recordings were obtained in artificial cerebrospinal fluid (ACSF). In the presence of tetrodotoxin to inhibit Na_V currents, only the slow depolarization is evoked by the same current step as above. In other experiments, Crandall and colleagues showed that the slow depolarization in these neurons is generated by T-type, Ca_V3 currents. *Adapted from Crandall et al. (2010) with permission from the Society for Neuroscience.*

Slow frequency oscillations of the membrane potential bring thalamic reticular neurons to threshold for firing fast Na_V-dependent action potentials and are generated by Ca_V3 channels. Ca_V3 channels have the unique property of activating at relatively negative voltages. The different contributions of Ca_V3 and Na_V channels are separable by the use of tetrodotoxin (a neurotoxin that selectively inhibits Na_V channels; Table 13.2). In the presence of tetrodotoxin, fast spikes are eliminated, leaving slower, longer lasting and smaller depolarizations (Fig. 13.5) (Crandall et al., 2010).

Delivering Calcium to Specialized Sites Triggered by Membrane Depolarization

Ca_V channels are present at specialized regions of cells that depend on depolarization-dependent calcium entry to trigger a cellular function. For example, Ca_V2 channels at presynaptic active zones deliver a bolus of localized calcium to the synaptic vesicle release

machinery, triggering exocytosis in response to membrane depolarization. The biophysical properties of presynaptic Ca_V channels influence the efficiency with which they couple membrane depolarization to calcium entry and subsequent transmitter release. $Ca_V2.1$ and $Ca_V2.2$ channels are present at most neuronal synapses and their dynamic properties influence the temporal features of synapses, including whether they facilitate or depress during trains of action potentials (Leal et al., 2012; Catterall et al., 2013).

Functions of Voltage-Gated Ion Channels Independent of Ion Flow

Certain VGICs function as voltage-sensors which couple directly to target proteins to mediate a conformational change, or which trigger an intracellular signaling cascade, independent of ion flow. For example, $K_V10.1$ channels identified in the fruit fly *Drosophila* and called ether-a-go-go (EAG) are known to regulate cell proliferation independently of their ability to conduct K^+ ions (Hegle et al., 2006). $K_V10.1$ signals through the mitogen-activated protein kinase (MAPK) pathway to increase p38 MAPK and to stimulate cell proliferation in a voltage-dependent way. Similarly, $Ca_V1.1$ channels trigger Ca^{2+}-dependent contraction of skeletal muscle, not by conducting Ca^{2+} ions across the muscle plasma membrane, but by triggering Ca^{2+} release from the sarcoplasmic reticulum (Schneider and Chandler, 1973; Rios and Brum, 1987; Tanabe et al., 1988). The skeletal muscle $Ca_V1.1$ channel binds directly to the ryanodine Ca^{2+} channel in the sarcoplasmic reticulum; the conformational change in $Ca_V1.1$ induced by membrane depolarization induces a conformational change in the ryanodine receptor that conducts Ca^{2+} across the sarcoplasmic reticulum membrane to the cytoplasm. In the case of $Ca_V1.1$, drugs that inhibit the ion pore do not interfere acutely with muscle contraction but drugs that impede the movement of the S4 voltage-sensors uncouple depolarization from contraction (Rios and Brum, 1987). The biophysical properties of the voltage-sensing domain of $Ca_V1.1$ and $K_V10.1$ control cellular responses but the flow of ions does not.

MEASURING BIOPHYSICAL PROPERTIES OF VOLTAGE-GATED ION CHANNELS

Each neuron expresses a myriad of functionally distinct ion channels. The membrane potential of a neuron depends on the relative conductance of the membrane to the major ions that flow through it, and their respective reversal potentials. You will read in other chapters that, in the absence of VGICs or strongly voltage-dependent conductances, the change in the membrane potential (ΔV) in response to a step-wise injection of current (I) can be reasonably well-predicted. The initial time course of the membrane potential follows a rising exponential that depends upon the membrane capacitance and input resistance ($\tau = R_m \cdot C_m$), and reaches a final steady-state value that depends upon the input resistance ($\Delta V = I \cdot R_m$). By contrast, the response of the membrane potential is dramatically different when the size of the current injection is increased to suprathreshold values in excitable cells (see Fig. 13.5). Suprathreshold membrane depolarizations recruit VGICs that in turn induce changes in the membrane potential that are no longer related to the shape or size of the square pulse of current that triggered the response. The most extreme example of this is the action potential, the initial phase of which is an explosive positive feedback cycle (Fig. 13.6): g_{Na} or g_{Ca} increases; the ensuing I_{Na} or I_{Ca} further depolarizes the membrane potential (ΔV); and membrane depolarization opens more Na_V or Ca_V channels, and so on. This positive feedback cycle continues until g_K starts to dominate over g_{Na} as K_V channels open and Na_V channels inactivate.

The interdependence of g, V, and I when VGICs are activated posed a significant challenge to early

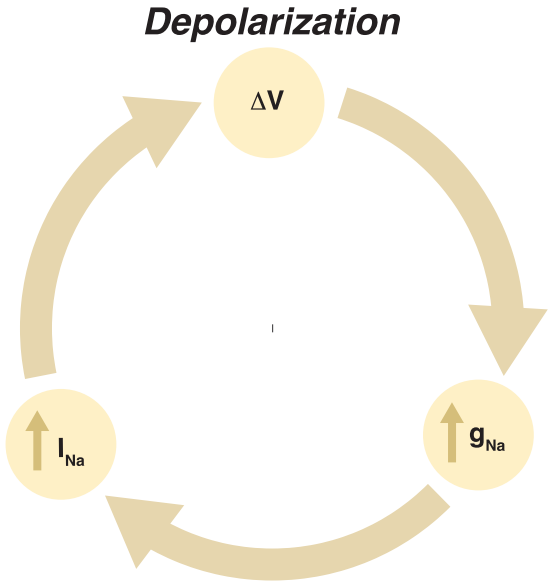

FIGURE 13.6 The cycle of regenerative depolarization triggered in excitable cells when Na_V or Ca_V channels are engaged. An initial depolarization of the membrane potential (ΔV), when applied from a relatively hyperpolarized voltage, triggers a rapid increase in the conductance of the membrane to Na^+ (g_{Na}) because Na_V channels open, Na^+ ions enter the cell (I_{Na}) leading to membrane depolarization and this depolarization opens more Na_V channels. This positive cycle repeats until Na_V channels inactivate and the conductance of the membrane to K^+ increases, because K_V channels open. Variations of this regenerative cycle of depolarization/Na_V channel activation have been published including by Bernard Katz in his wonderful 1966 book on "Nerve, muscle, and synapse" (Katz, 1966).

biophysicists in their quest to determine the ionic basis of suprathreshold changes in the membrane potential. Specifically, biophysicists wanted to observe and quantify the voltage and time-dependent changes in the conductance of the plasma membrane to Na^+ and K^+ ions (g_{Na} and g_K) that they believed gave rise to the action potential:

$$g_{Na} = \frac{I_{Na}}{(V_m - E_{Na})} \tag{13.1}$$

$$g_K = \frac{I_K}{(V_m - E_K)} \tag{13.2}$$

where g_{Na} and g_K are membrane conductance (siemens) to Na^+ and K^+; E_K the K^+ equilibrium potential (V); E_{Na} the Na^+ equilibrium potential; V_m the membrane potential (V), and I_{Na} and I_K membrane currents.

The voltage-clamp recording method, first applied to measure membrane currents in squid giant axon by Kenneth S. Cole in the USA and Sir Alan L. Hodgkin, Sir Andrew F. Huxley and Sir Bernard Katz in the UK, was a major technical breakthrough toward that goal. Currents flowing through VGICs in squid axon that generate the action potential were measured at different voltages, and with high temporal resolution. An electrode—silver wire—inserted into the center of the squid axon and external electrodes connected to a feedback amplifier automatically supply current to maintain the membrane potential at the desired level. When VGICs open, the current that flows through them is rapidly balanced by an equal and opposite current supplied by the voltage-clamp. Thus, current flow across the membrane is measured at constant voltage. Capacitative currents only flow when the membrane potential is changing; therefore, under voltage clamp, these currents are transient and restricted to the start of the voltage step.

The importance of the landmark publications in the *Journal of Physiology* by Hodgkin, Huxley and colleagues starting in 1949 and including the seminal papers of 1952 are described in detail in Chapter 14. Among their many achievements, Hodgkin and Huxley measured experimentally, and derived formal relationships to describe, the time-dependent and voltage-dependent changes in g_{Na} and g_K. The quantitative models derived by Hodgkin & Huxley developed using extensive experimental data are still used today. The following equation relates total ionic current across the membrane to the sum of the individual membrane currents.

$$I = C_m \frac{dV}{dt} + \bar{g}_K\, n^4 (V_m - E_K) + \bar{g}_{Na}\, m^3 h (V_m - E_{Na}) + \bar{g}_L (V_m - E_L) \tag{13.3}$$

where C_m is the membrane capacitance (in farads); g_K the maximum membrane conductance (in siemens) to K^+; g_{Na} the maximum membrane conductance to Na^+; n, m, and h are time and voltage dependent gating variables: n the probability of one K_V channel activation gate being in a permissible position for channel opening, and n^4 is the probability of all four activation gates being in the permissive position, m is the probability of one Na_V channel activation gate being in the permissible position for channel opening, m^3 is the probability of all three being in the permissive position, and h is the probability of the inactivation gate being in the permissive position (and $1 - h$ is the probability that the inactivation gate is in the nonpermissive position); E_K is the K^+ equilibrium potential (V); E_{Na} the Na^+ equilibrium potential; and E_L the reversal potential for current flow through the leak.

Axonal Na_V and K_V currents elicited by a voltage step to 0 mV, using the Hodgkin-Huxley model, are shown (Fig. 13.7). Only I_{Na} and I_K currents are illustrated and capacitative and leak currents are omitted. Capacitative currents are constant, and leak currents in many cells and neurons are approximately linear over the range of recording. They are typically subtracted from the recordings to isolate VGICs, thus the total current (I_{Total}) shown is the sum of individual I_{Na} and I_K.

$$I_{Total} = I_{Na} + I_K \tag{13.4}$$

The time-dependent changes in I_{Total}, I_{Na} and I_K elicited by a square test pulse to 0 mV reflect changes in g_{Na} and g_K. It is important to emphasize that the currents measured in voltage clamp during the test pulse are under *constant* voltage.

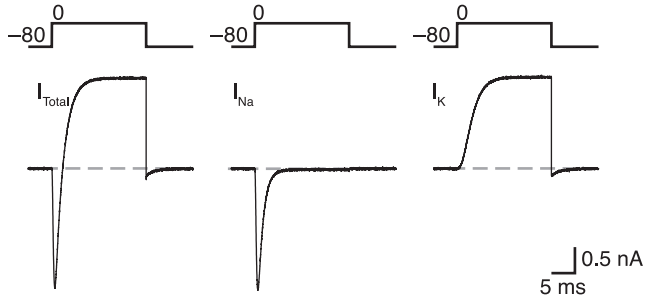

FIGURE 13.7 Simulated Na_V and K_V currents generated using the Hodgkin and Huxley model that relates total ionic current across the membrane to the sum of the individual membrane currents (Hodgkin & Huxley, 1952) (Equation 13.3). A voltage step to 0 mV is applied from a holding potential of −80 mV and total current (I_{Total}), I_{Na} and I_K are shown. For simplicity, leak currents are not included in the simulation. A rapidly developing transient inward Na^+ current is followed by a more slowly developing but sustained outward K^+ current. *Simulations are courtesy of Erin Hoops (Brown University, Providence, RI).*

The currents shown illustrate several important biophysical features of VGICs:

- *Voltage-dependent activation of Na_V and K_V channels* at depolarized membrane potentials arise from the rapid increase in channel open probability P_{open} that is preceded by an increased likelihood of finding activation gates and inactivation gates in the position permissible for channel opening (m, h, n).
- *Net inward I_{Na} at 0 mV* because the driving force on Na^+ ($V_m - E_{Na}$) is $\sim +60$ mV.
- *Net outward I_K at 0 mV* because the driving force on K^+ ($V_m - E_K$) is ~ -90 mV.
- *Rapid Na_V channel activation kinetics* relative to the slower activation kinetics of K_V channels accounts for the initial inward Na^+ current that underlies the initial depolarization phase of the action potential.
- *Sigmoidal activation kinetics* of I_{Na} and I_K immediately follow membrane depolarization (most apparent for I_K because of its slower activation kinetics) is consistent with the requirement that multiple activation gates must be in the permissible position for the channels to open.
- *Rapid decrease in I_{Na} during constant voltage* at 0 mV is consistent with the movement of an inactivation particle to a position that is not permissible for ion flow through Na_V channels.
- *Sustained I_K during constant voltage* at 0 mV suggests the absence of a rapid mechanism to inactivate this class of axonal K_V channel during prolonged depolarization.

STEADY-STATE CURRENT-VOLTAGE RELATIONSHIPS

The steady-state current-voltage relationships of axonal Na_V and K_V channels are shown in Chapter 14. Here we illustrate voltage-clamp recordings of whole cell Ca_V2 currents that are overall very similar to Na_V currents (Fig. 13.8). At test voltages between -40 mV and $+50$ mV the net flow of I_{Ca} is inward (negative); as the test voltage increases to values between -40 mV and 0 mV I_{Ca} increases in amplitude; at $\sim$0 mV I_{Ca} reaches a maximum value; at test voltages positive to $\sim$0 mV I_{Ca} decreases until it reverses direction at voltages positive to $\sim +60$ mV; and at test voltages positive to $+60$ mV net I_{Ca} is outward (Fig. 13.8A, B).

The elementary components that determine current amplitude at steady state are: N, the number of channels available to open; i, the amplitude of current that flows through a single channel (which is a function of voltage and typically in the pA range); and P_{open}, the average channel open probability which is a function of voltage and time.

$$I_{Ca} = N\, P_{open}\, i \tag{13.5}$$

To extract steady state P_{open} from recordings of macroscopic currents, the other variables, N and i, must be measured or held constant. It is not possible to measure the total number of channels N directly from macroscopic currents but N can be kept constant during a typical voltage-clamp experiment. For VGICs that inactivate, it is critical that the same numbers of channels are available for opening at the start of each test potential. This condition can be met by returning the membrane potential to a hyperpolarized value between each test depolarization, thereby allowing VGICs to recover from inactivation and to return to the closed state (i.e., in state C_0 in Fig. 13.9). (Steady state P_{open} values are not reached during test pulses that induce rapid inactivation of VGICs, but peak currents are used to approximate steady-state current-voltage relationships.)

Note that i (pA) is the product of the single channel conductance γ (pS) and the driving force ($V - E_{Rev}$). Here, γ is a measure of the ease with which ions flow through single open channels; γ depends on the intrinsic properties of the ion pore and the number of permeant ions available. The single channel conductance and current can saturate at high rates of ion flow. The direction of current flow at a given membrane potential depends on the potential at which current through the ion channel reverses direction, E_{Rev}, which in turn depends on the permeation properties of the ion pore.

$$i_{Ca} = \gamma(V_m - E_{Rev}) \tag{13.6}$$

The driving force on Ca^{2+} ions decreases as the membrane potential (V_m) is depolarized and as it approaches the Ca_V channel E_{Rev}. Ca_V is strongly selective for Ca^{2+} provided that there is sufficient Ca^{2+} to occupy binding sites within the pore (Kd $\sim$1 μM; see below) but the current reverses direction at membrane voltages close to $+60$ mV, significantly less depolarized than the Nernst equilibrium potential for calcium under normal physiological solutions ($E_{Ca} \sim 120$ mV) (Fig. 13.8D). The unexpected reversal potential for Ca_V channels is explained by the finding that they permit the flow of cations (normally K^+ but also Cs^+) *outward* through the central ion pore.

Note that i and γ cannot be measured directly by recording macroscopic currents but, as discussed in the following section, they can be measured from membrane patches (although elegant methods have been used to derive i and γ indirectly by nonstationary fluctuation analyses of macroscopic VGIC currents). But I and P_{open} can be measured at different membrane potentials from

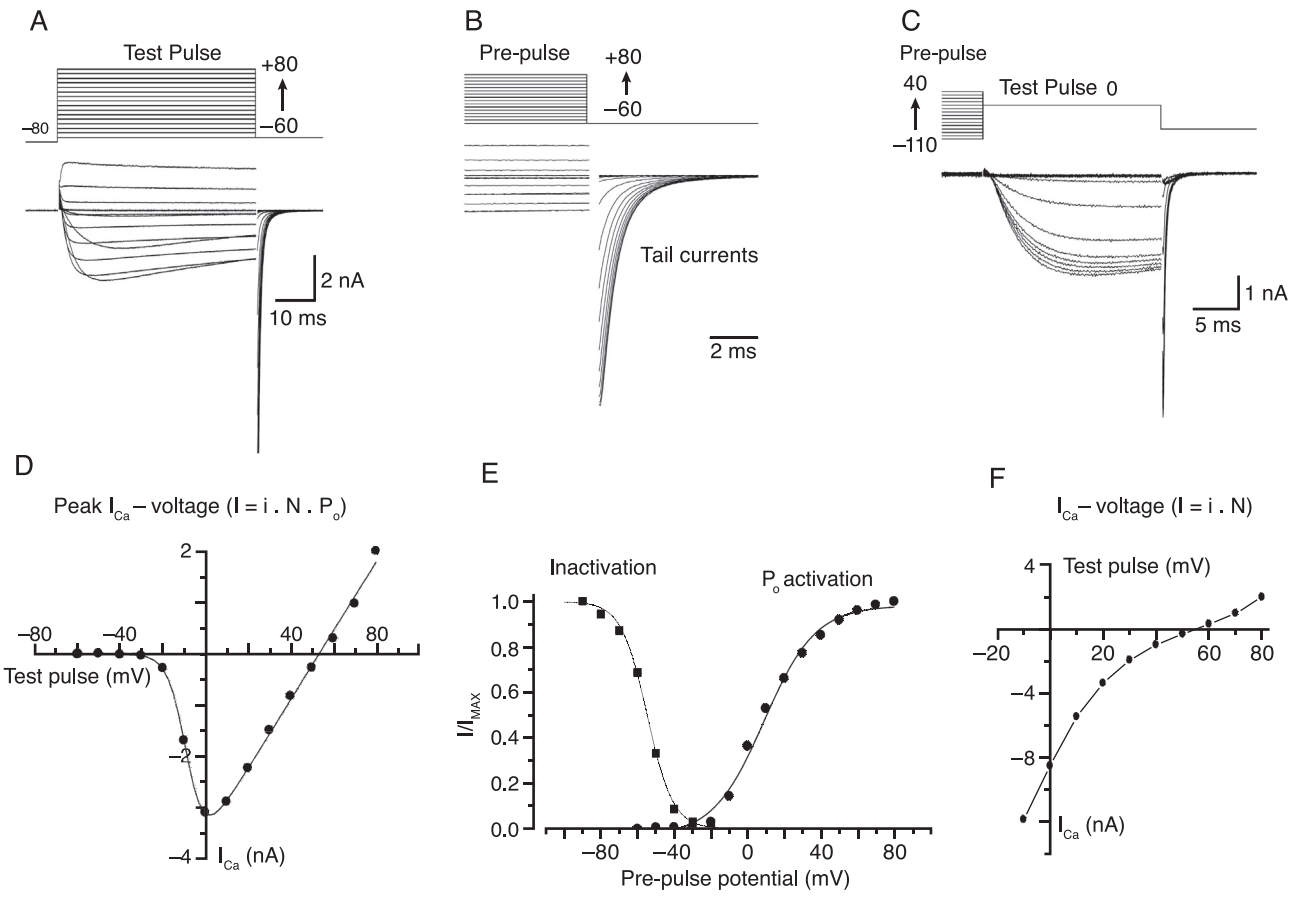

FIGURE 13.8 Whole cell calcium currents recorded from a tsA201 mammalian cell line transiently expressing human $Ca_V2.2$ cDNA together with auxiliary subunits. Currents were recorded with 1 mM extracellular Ca^{2+} as the charge carrier. **A**, Ca_V currents were evoked by a series of test pulses to voltages between −60 mV and 80 mV applied in 10 mV increments from a holding potential of −80 mV. Deactivation tail currents were measured at −60 mV. **B**, Series of tail currents shown on an expanded time scale from recordings shown in **A**. **C**, Series of calcium currents activated by a test pulse to 0 mV immediately following a series of 2 s prepulses to holding potentials between −110 mV and 40 mV applied in 10 mV increments. **D**, Peak calcium channel current densities (pA/pF) at various test potential from data shown in **A**. I-V relationships were fit to data from individual cells using the product of the Boltzmann function and a linear line to estimate activation midpoint ($V_{1/2}$), slope factor (k) and reversal potential (V_{rev}). $V_{1/2} = 3.7$ mV, $k = 4.3$ mV and $V_{rev} = 53$ mV. **E**, Activation plots obtained from currents shown in **B**, obtained from tail current amplitudes at −60 mV at the end of 25 ms duration test pulses. Normalized tail currents at −60 mV (I/I_{max}) plotted against test pulse were fit with Boltzmann functions $V_{1/2} = 14$ mV and $k = 8.9$ mV. Steady-state inactivation relationships from normalized peak current amplitudes at 0 mV following 2-s prepulse steps applied in 10 mV increments to potentials between −110 mV and 0 mV (shown in **C**). The inactivation curve was fit with a single Boltzmann $V_{1/2}$: −54 mV and $k = 7$ mV. **F**, Instantaneous current-voltage relationship derived from peak current voltages in **A** and the activation curve in **E**. *Data courtesy of Arturo Andrade (Brown University, Providence, RI).*

macroscopic tail currents at hyperpolarized membrane potentials immediately following a test pulse. Tail currents are generated at hyperpolarized voltages when Ca_V channels are opened by a preceding depolarization (Fig. 13.8D). This is because Ca_V channels, and all VGICs, do not close the instant that the membrane is hyperpolarized, but the change in the driving force is instantaneous.

Provided that Ca_V channels do not reopen at −60 mV, the time course of the tail current reflects the rate of channel closing (s^{-1}) or the average length of time (s) the channel is open at −60 mV. The tail current I_{tail} increases as the test pulse increases but then saturates (Fig. 13.8B and 13.8E). Because I_{tail} is measured at the same membrane potential, the driving force, and consequently i, are constant. Under these conditions:

$$P_{open} = \frac{I_{tail}}{I_{max}} \tag{13.7}$$

where I_{tail} is normalized to the maximum tail current (I_{max}).

The ability to step the membrane voltage from one value to another, essentially without a delay, is critical for these experiments. The relationship between P_{open} and the test pulse is the activation curve for Ca_V channels (Fig. 13.8E). Similar protocols can be used to determine the voltage-dependence of activation of macroscopic Na_V and K_V channel currents. The steady

state P_{open} or activation of VGICs is described by the Boltzmann function:

$$P_{open} = \frac{1}{1 + \exp[(V_{50} - V_m)/k]} \tag{13.8}$$

where V_{50} is the voltage at the midpoint of activation, V_m is the membrane potential, and k is the slope and is related to the equivalent number of charges that move in the electric field during activation (Fig. 13.8E).

As demonstrated by Hodgkin and Huxley and described in Chapter 14, tail currents can also be used to extract instantaneous current-voltage relationship of open channels; in this case I_{tail} currents are measured at different voltages (different driving forces) but the preceding depolarization used to activate the channels is the same (constant P_{open}). Using this approach, Hodgkin and Huxley showed that the relationship between current through open Na_V and K_V channels ($i \cdot N$) and membrane voltage were ohmic: i.e., γ is constant over the voltage range studied allowing g_{Na} and g_K to be derived according to the general equation of Equations 13.1 and 13.2,

$$g = \frac{I}{(V_m - E_{rev})} \tag{13.9}$$

where $g = N \cdot \gamma$, γ is the single channel conductance (typically pS), N is the number of channels available, I the macroscopic current (typically nA for a neuron), V_m the membrane potential, and E_{rev} is the channel current reversal potential. In the example shown in Fig. 13.8C, the instantaneous current ($N \cdot i$) at different voltages derived from measuring the peak Ca_V current amplitudes (I_{Ca}), and measuring P_{open} from tail currents, is not ohmic but it rectifies (see the following). Therefore, the voltage dependence of γ has to be incorporated in models of time dependent and voltage dependent changes in g_{Ca} during, for example, an action potential or a series of action potentials.

The steady state voltage-dependence of channel inactivation can be measured using a prepulse voltage-clamp protocol (Fig. 13.8C and 13.8E). Prepulses to a range of voltages are applied long enough for inactivation to reach steady state, prior to a test depolarization to activate the channels (0 mV in Fig. 13.8E). As the prepulse is stepped to more depolarized voltages, more channels enter an inactivated state. The voltage-dependence of inactivation is also fit with a Boltzmann function (Fig. 13.8E).

The time-dependent increases in g_{Na} and g_K elicited by membrane depolarization follow sigmoidal, not exponential functions that would be expected of a single two-state model. The S-shaped or sigmoidal activation time course of K_V currents is illustrated in Fig. 13.7. Na_V and Ca_V channels have similar sigmoidal activation kinetics, although overall they open more quickly compared to axonal K_V channels illustrated in Fig. 13.7. Based on their original observations, Hodgkin and Huxley concluded that g_{Na} and g_K activation were best described by a process that invoked multiple voltage and time-dependent charged particles in Na_V and K_V channels that had to move to permissible positions to permit channel opening (illustrated in Fig. 13.9). An additional inactivation particle was required to model g_{Na}. Three activation charge particles (gates) and one inactivation gate for Na_V, and four activation gates for K_V had to be in the permissible position for the channels to open. The movements of activation and inactivation gates were assumed to be voltage-dependent. The probability that a Na^+ channel is open can therefore also be described according to the following:

$$P_{open} = m^3 h \tag{13.10}$$

where m is the probability of one Na_V channel activation gate being in the permissible position for channel opening, m^3 is the probability of all three being in the permissible position, and h is the probability of the inactivation gate being in the permissive position ($1 - h$ is the probability that the inactivation gate is in the nonpermissive position). Similarly, the probability that a K_V channel is open can be described according to the following:

$$P_{open} = n^4 \tag{13.11}$$

where n is the probability of one K_V channel activation gate being in a permissible position for channel opening, and n^4 is the probability of all four activation gates being in the permissive position.

I_{Na} depends on the channel open probability, the number of Na_V channels available to open N, and the amplitude of single Na_V channel currents i.

$$I_{Na} = N\, P_{open} i \tag{13.12}$$

Expressed in terms of single channel conductance, γ, and driving force ($V - E_{Na}$),

$$I_{Na} = N\, P_{open}\, \gamma (V - E_{Na}) \tag{13.13}$$

The conductance g_{Na} is equivalent to the product of N and γ,

$$I_{Na} = g_{Na} P_{open} (V - E_{Na}) \tag{13.14}$$

Expressed in terms of charged gating variables and maximum conductance, m, h, and n are functions of time and voltage illustrating the origin of the Hodgkin-Huxley equation shown previously:

$$I_{Na} = \overline{g}_{Na}\, m^3 h\, (V_m - E_{Na}) \tag{13.15}$$

Subsequent biophysical analyses, direct measurements of single channel currents, and high-resolution ion channel structures support the essential elements of the Hodgkin and Huxley formalizations.

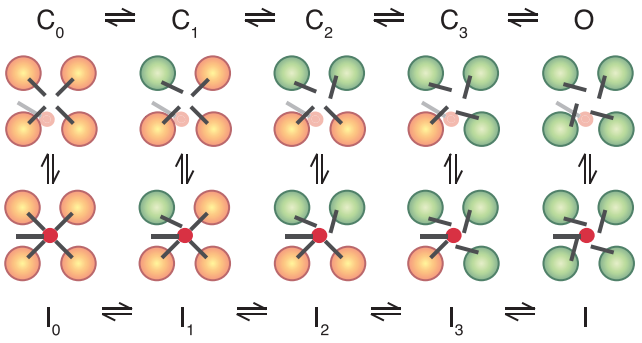

FIGURE 13.9 Minimum number of distinct conformational states needed to account for the voltage and time-dependent activation, deactivation and inactivation properties of Na_V, Ca_V and K_V channels. Axonal, noninactivating K_V channels are described by four closed states (C0, C1, C2, C3) and a single one open state (O) (top row). Four domains DI–DIV (Fig. 13.1A), are represented by yellow and green circles. Yellow represents domains in which the S4 is in the resting state (nonpermissible for channel opening). Green represents domains in which S4 has moved to the active state (permissible for channel opening). S4-activation gates of each domain are depicted by black bars. All four activation gates must be in the permissible position for channels to open. Only one gate is required to move back to the nonpermissible position for the channel to close. Na_V, Ca_V, and several other types of K_V channels inactivate. An inactivation particle is depicted by the black bar; it has a red ending that occludes the central ion pore. The movement of this inactivation particle is sufficient to prevent ion flow. Inactivation can occur from all four closed states as well as from the open state.

Figure 13.9 illustrates the transitions in VGICs that were predicted to occur during activation, deactivation and inactivation according to the Hodgkin-Huxley model of axonal Na_V and K_V channel properties. The model includes four closed conformations where 0, 1, 2, or 3 activation gates are in the permissible position for channel opening; a single open state when all four activation gates are in the permissible position; and five inactivation states that lead from each of the four closed states and one open state that have a single inactivation particle occluding the ion pore. This kinetic scheme also accounts for the ability of many VGICs to inactivate from the closed state (independent of channel opening).

The Expected and Actual Reversal Potential for Current Flow Through Ca_v Channels

The reasons for the asymmetry in Ca^{2+} ion selectivity through Ca_V channels based on direction of current flow is two-fold: first, the difference in free Ca^{2+} concentration between the outside and inside of a cell is extremely large, 20,000-fold, and much larger than the concentration gradients that exist for Na^+ and K^+ across the plasma membrane. A large asymmetry in the concentration of a permeant ion imposes a nonlinearity on current flow that is predicted from the Goldman Hodgkin Katz (GHK) current equation and is observed experimentally. The GHK equation predicts that the effective resistance to ion flow across the membrane is lower when ions flow from the side of high concentration (more ions) compared to when ions flow from the side of low concentration (fewer ions) (Hille, 2001). Second, the selectivity filter in many Ca_V channels depends crucially on the presence of Ca^{2+} itself. In Ca_V1 and Ca_V2 channels, Ca^{2+} binds within the ion pore preventing other cations from entering. Early biophysical studies described the anomalous mole fraction effect because ion flow through these Ca_V channels does not follow the predicted relationship but is bell-shaped (described in more detail in Fig. 13.15) (Hess and Tsien, 1984; Hess et al., 1986). In the absence of extracellular Ca^{2+} certain Ca_V channels become nonselective to many cations. The Ca^{2+} binding site(s) within the ion selectivity filter can be titrated with increasing concentrations of extracellular Ca^{2+} and has an estimated Kd ~ 10 μM (Hess and Tsien, 1984; Hess et al., 1986). The concentration of Ca^{2+} is so low inside the cell that the occupancy of Ca^{2+} at these binding site(s) is relatively short, permitting the flow of K^+ (or other monovalent cations) outward through the ion channel pore. Inward flow of monovalent cations (such as Na^+) is occluded because sufficient Ca^{2+} (2 mM) is outside to occupy the binding sites within the pore a high fraction of the time.

VOLTAGE-CLAMP RECORDING METHODS TO STUDY BIOPHYSICAL PROPERTIES OF VGICS

The voltage-clamp recording method made it possible to determine the precise relationship between membrane current, membrane conductance, and membrane voltage, and consequently to derive a quantitative description of the ionic basis of the action potential. Several variations of the voltage-clamp recording method were subsequently developed to resolve single ion channel currents, and to measure ion channel currents in a range of cells including neurons and in specialized regions of cells including presynaptic terminals and dendritic spines. All voltage-clamp recording methods have the following common features:

- The membrane potential of a whole cell or an electrically isolated patch of membrane is held constant at predetermined values—at constant potential.

- The membrane potential of a whole cell or an electrically isolated patch of membrane is continuously monitored and compared to the desired membrane voltage (command voltage) via a feedback amplifier.
- Any difference between the command voltage and measured membrane voltage is amplified at the output of the feedback amplifier. This output controls the amplitude, polarity, and time course of current required to maintain constant potential.
- The amplitude and time course of the current required to maintain the membrane potential at the command voltage is equal and opposite to the membrane current.
- Under ideal experimental conditions, sufficient current can be applied with sufficient speed to clamp the membrane potential of the cell or an electrically isolated patch membrane as various ion channels open and close. However, constant voltage is often not achieved in recordings of rapidly activating VGICs such as Na_V channels.

The two-microelectrode voltage clamp recording method was introduced to measure membrane currents in a variety of large cells including muscle cells, oocytes, and neurons of $>\sim 40\,\mu m$ diameter that remained viable after impalement with two microelectrodes (Hille, 2001). The two-microelectrode voltage-clamp recording method uses one electrode to continually monitor the membrane voltage and a second electrode to inject currents. However, most neurons in nervous systems from *C. elegans* to humans are too small for two-microelectrode recording. This significant technical hurdle was all but eliminated following the introduction of the whole cell patch-clamp recording method as discussed below (Sigworth, 1986; Hamill et al., 1981).

The Patch-Clamp Revolution

In 1976, Bert Sakmann and Erwin Neher published the first recordings of currents flowing through single ion channels in a living cell (Neher and Sakmann, 1976). Until their recordings, various indirect—although incredibly elegant—approaches had been used to estimate the unitary properties of ion channels from recordings of macroscopic currents. The currents of extrasynaptic ACh receptor (AChR) cation channels in frog muscle were only ~ 3.5 pA in size, but they resolved these currents by electrically isolating a small patch of membrane and significantly limiting other extraneous signals (noise). Neher and Sakmann achieved this by pushing the tip of a glass electrode, with an open tip diameter of $3-5\,\mu m$ and smoothed by fire polishing, up against the surface of the muscle (see Figs. 13.10, 13.11 and Fig. 13.14 for examples of single Ca_V channels). In their recordings, the electrode was filled with extracellular solution and an agonist to activate AChRs. It was connected to a virtual ground circuit to maintain the potential of the inside of the electrode, using an operational amplifier and a high resistance feedback resistor to measure membrane current. To maintain constant voltage in the muscle cell, in their early recordings, Neher and Sakmann also used a two-microelectrode voltage-clamp circuit simultaneously while recording single channel currents using the patch electrode (Neher and Sakmann, 1976).

In 1980, Neher and Sigworth described an improvement to the patch clamp recording method that increased the signal-to-noise ratio, resulting in substantially improved temporal resolution (Sigworth and Neher, 1980). They applied gentle suction inside the recording pipette when it was pressed against the cell membrane (see Fig. 13.12). This action increased the seal resistance between pipette and cell membrane substantially (from $10^8\ \Omega$ to $10^{10}\ \Omega$). The higher seal resistance improved the signal-to-noise ratio and also made it possible to apply voltage steps to the inside of the patch electrode, without the need to voltage-clamp the entire cell with microelectrodes. In addition to achieving seal resistances of $>1\,G\Omega$, they also decreased stray capacitance from the electrode wall by coating the outside of the recording pipette with Sylgard® (silicon elastomer).

The single channel conductance (γ) can be calculated from Ohm's Law as shown for macroscopic currents in Equation 13.9:

$$\gamma = \frac{i}{(V_m - E_{Rev})} \tag{13.16}$$

where γ = single channel conductance (S); i = single channel current amplitude (A); V_m = the membrane voltage (V); and E_{Rev} = is the potential at which current flow through the channel reverses direction (V). Single channel conductances of most VGICs typically fall in the range of 1 pS to 40 pS but these values depend on the concentration of permeant ion used to record single channel activity. For example, high extracellular Ba^{2+} is often used in the patch pipette rather than 2 mM Ca^{2+} as the charge carrier to resolve single Ca_V channel currents and maximize the rate of ion flow (see Figs. 13.11 and 13.14; and see the following). For many ion channels, the single channel conductance depends on voltage, which can be seen from nonlinearity in single channel current-voltage relationships.

The average activity of single channel currents recapitulates the time course of the whole cell Ca_V currents (see Fig. 13.11). The stochastic nature of ion channel

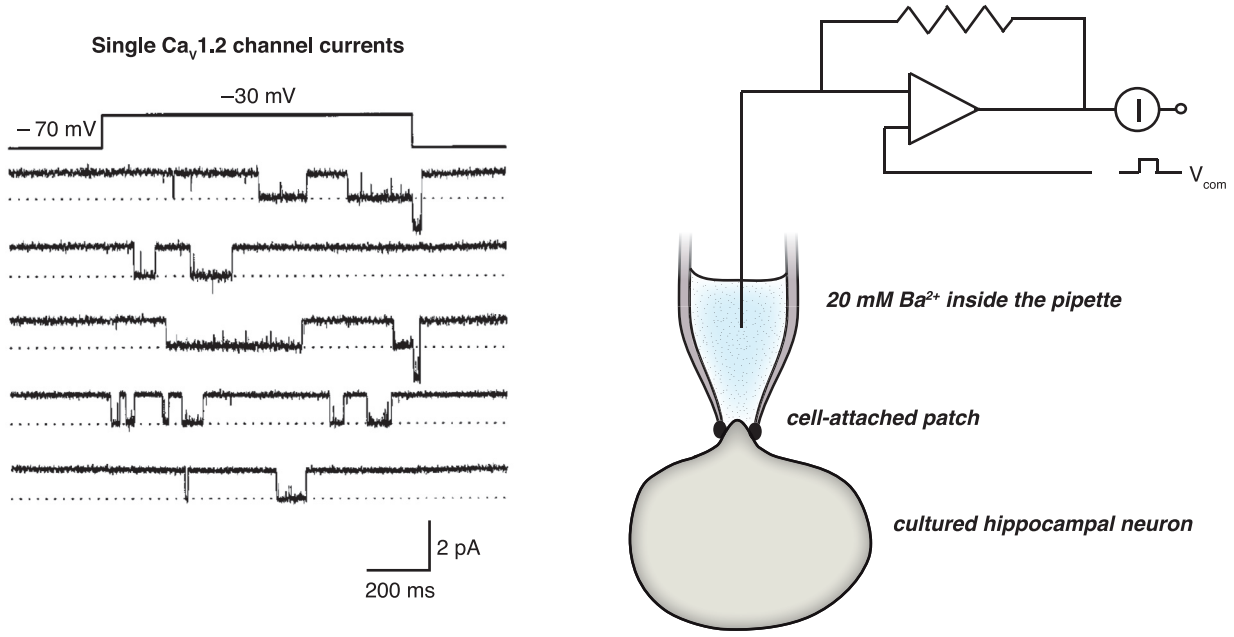

FIGURE 13.10 Single Ca_V1 channel currents recorded from a cell-attached membrane patch. Single channel currents recorded from hippocampal neurons using 20 mM Ba^{2+} as the charge carrier. Cell-attached patch recordings were obtained in the presence of an agonist FPL 64176 that is known to prolong the openings of these Ca_V1 ion channels. The single channel current amplitude is ~1 pA at −30 mV. Large tail-current openings are observed in the first and third sweeps. Channels remain open the instant the membrane voltage is returned to −70 mV, this increases the driving force for ion flow through the channel and therefore the single channel current amplitude is much larger (see Equation 13.16). The channels close within a few milliseconds after the membrane voltage is returned to −70 mV. The dashed line indicates the open state of the channel. Recordings were reproduced from reference (Schjott and Plummer, 2000) with permission from the Society for Neuroscience. The cell-attached patch clamp recording arrangement is shown to the right of the recordings. In these experiments, the neurons are placed in isotonic K^+ together with 5 mM EGTA to remove extracellular calcium. This solution effectively clamps the membrane potential at 0 mV and the presence of EGTA prevents calcium toxicity. The voltage is held constant inside the patch electrode and the applied voltage (extracellular in the patch pipette) is equal and opposite to the desired voltage on the inner side of the patch of membrane.

gating dictates that it is not possible to predict if a channel will be open or closed at any point in time, but the average activity of a homogenous population of ion channels can be measured. For example, the latency to the first Ca_V channel opening is not predictable for any single sweep in Figs. 13.10, 13.11 and Fig. 13.14, but the average time to first opening is predictable at a given membrane voltage.

In 1981 Owen Hamill, Alain Marty, Erwin Neher, Bert Sakamann and Fred J. Sigworth published a remarkable series of recording configurations illustrating the full utility of the patch-clamp recording technique (Hamill et al., 1981) (see illustration in Fig. 13.12). Starting with the formation of a high resistance seal between patch pipette and cell membrane (cell-attached), these investigators demonstrated that several different types of recording configurations could be achieved because of the remarkable mechanical stability of the electrical "gigaohm seal" even when excised from the cell. An inside-out patch is formed by rapidly withdrawing the pipette from the cell after gigaohm seal formation; the inner surface of the patch of membrane is exposed to the outside bath solution (Fig. 13.12). The inside-out patch recording method (i) gives access to the cytoplasmic surface and control of the composition of solution and, (ii) achieves complete electrical isolation from the cell allowing precise control of the voltage of the patch of membrane (Horn and Patlak, 1980; Hamill et al., 1981). Inside-out patches are also used to assess the action of intracellular signaling molecules on ion channels. For example, Mark Shapiro and colleagues showed that an analog of PIP_2 (diC8-PIP_2) strongly augments $K_V7.2/K_V7.3$ channel currents by increasing channel open probability in a dose-dependent manner (Fig. 13.13) (Li et al., 2005). If intracellular PIP_2 is not supplied to the inside of the patch, $K_V7.2/K_V7.3$ channel activity runs down rapidly in inside-out patches, an observation that has been reported for several other VGICs.

Hamill et al. (1981) also demonstrated how to form an "outside-out patch": an excised patch of membrane with the extracellular surface facing the bath solution

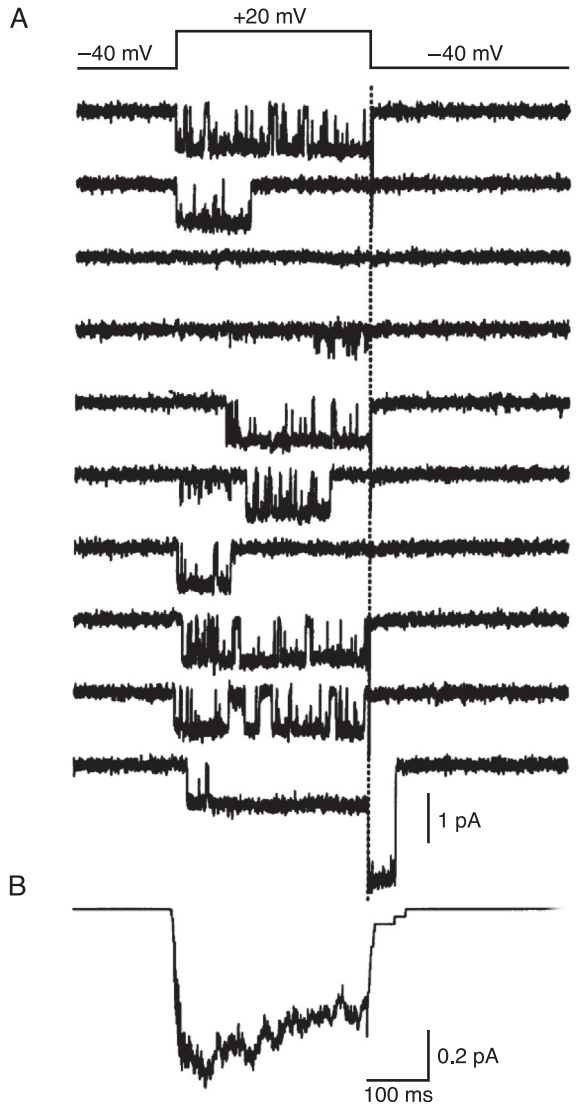

FIGURE 13.11 Single Ca_V1 channel currents recorded from a cell-attached patch. Single channel currents recorded from hippocampal neurons using 20 mM Ba^{2+} as the charge carrier. Recordings were made with the Ca_V1 agonist, (+)-(S)-202-791, present. **A**, Consecutive single channel openings are shown in response to a depolarization to +20 mV from a holding potential of −40 mV. The openings during the depolarization are ~1 pA. The vertical dotted line shows the precise time when the test pulse ends and the membrane potential returns to −40 mV. There is a large tail current present in the tenth sweep just as the membrane potential is returned to −40 mV, which is ~2.5 pA. **B**, The ensemble current from averaging 80 sweeps is shown below the individual traces. The ensemble resembles the whole cell current and shows that, on average, Ca_V1 channels inactivate during the step depolarization. *Recordings were adapted from Kavalali and Plummer (1994) with permission from John Wiley & Sons Ltd.*

(Fig. 13.12). Following giga-seal formation the patch of membrane is ruptured with strong suction in the patch pipette, the pipette is then withdrawn from the surface of the cell and as the patch is excised from the cell, the membrane sometimes reseals but now with the extracellular side of the membrane facing the bath. The outside-out recording configuration can be used to monitor currents through single channels that are activated by extracellular ligands.

Finally, and by far the most widely utilized recording configuration described in Hamill et al. (1981), is whole-cell recording (Fig. 13.12). In this configuration, the single patch electrode is used to control the membrane voltage (under ideal conditions) and to measure the aggregate membrane currents of the whole cell. After forming a gigaohm seal, the patch of membrane is ruptured by suction in the pipette giving physical as well as electrical access to the inside of the cell. As the membrane is ruptured, there is a large increase in the capacitance reflecting the addition of the whole cell membrane capacitance to the circuit. For cells of ~10−15 μm in diameter the membrane capacitance is ~5−10 pF (Hamill et al., 1981; Fenwick et al., 1982a; Fenwick et al., 1982b). A series of whole cell Ca_V currents evoked by a series of step-depolarizations in 10 mV increments are shown in Fig. 13.8A. Ca_V currents activate and inactivate with faster kinetics as the size of the voltage step increases.

Whole-cell recording was developed to measure currents from neurons that were too small for conventional two-microelectrode voltage-clamp recording, and it is by far the most used method to monitor currents in neurons and many other types of cells. Whole-cell recording is advantageous for several reasons:

- The seal resistance between cell membrane and electrode is high; and electrical access resistance between the electrode and the cell is low compared to the resistance of the recording electrode. Therefore, one low resistance electrode can be used to control voltage and record ion channel currents simultaneously from small neurons.
- The composition of the intracellular—through diffusional exchange between pipette and cell—and extracellular environments of the cell can be controlled. This allows for ion substitutions to isolate currents previously obscured in the total whole cell current; for example Na_V and Ca_V currents can be readily isolated from K_V channel currents by replacing K^+ with Cs^+ in the intracellular (pipette) solution (e.g., Fig. 13.8).
- Under ideal recording conditions, the temporal resolution and signal-to-noise ratio of currents measured by whole-cell voltage-clamp from small neurons are superior to two-microelectrode voltage-clamp recording, permitting resolution of very rapid and small events such as gating pore currents (Fig. 13.4).

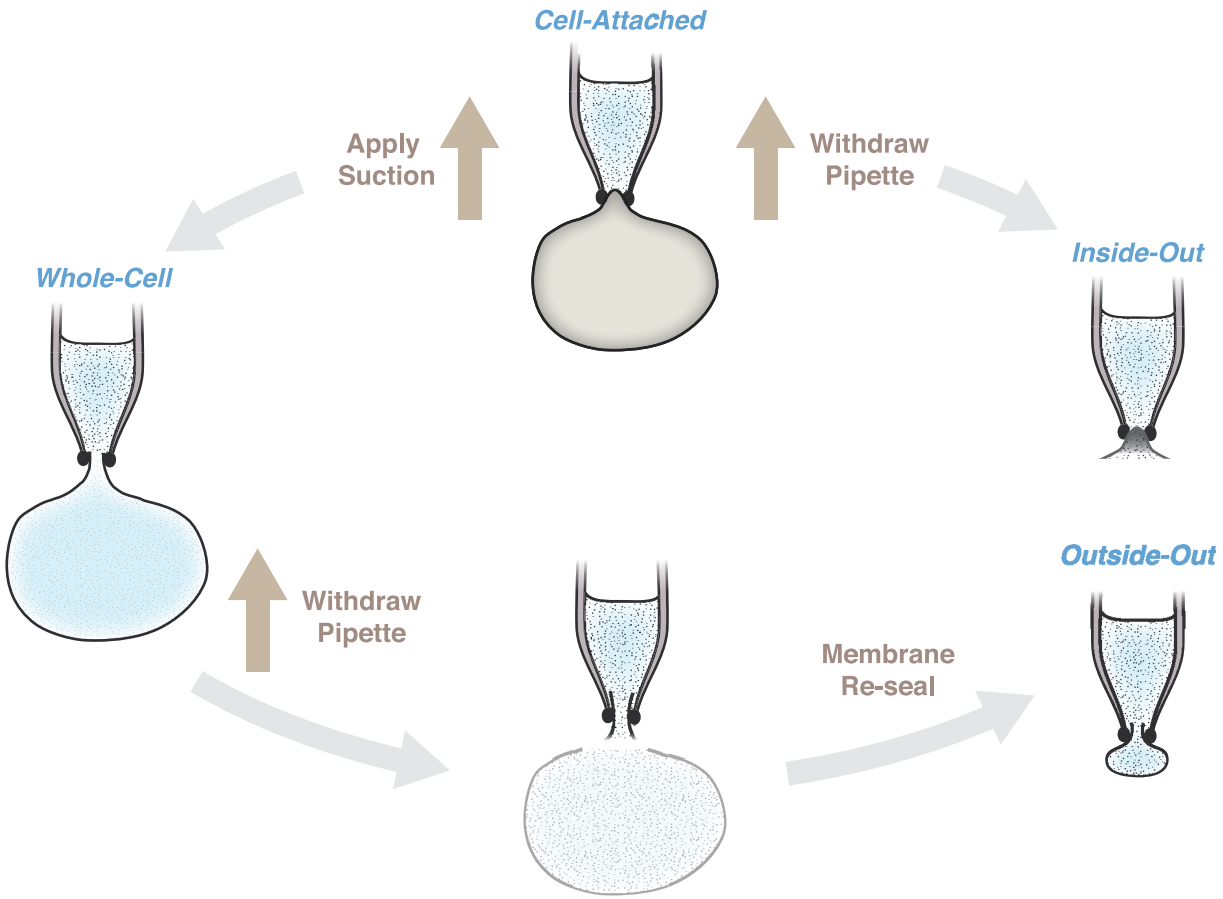

FIGURE 13.12 Different recording conformations using the patch-clamp method. The patch-clamp recording method, originally used to monitor single channel currents in cell-attached patches, is highly versatile (Hamill et al., 1981; Sigworth and Neher, 1980; Sigworth, 1986). As described in detail by Hamill et al. (1981), the first step in all recording configurations is the formation of a gigaohm seal. This high resistance seal greatly limits current flow between the inside of the patch pipette and the bath. In cell-attached patch recordings, currents through single ion channels can be resolved (see Figs. 13.14, 13.15) or, depending on the size of the patch electrode and the density of ion channels in the membrane, currents through a large number of ion channels (macropatch). The gigaohm seal between the patch pipette and the cell membrane is electrically as well as mechanically stable. The patch pipette can be withdrawn and, if the gigaohm seal remains intact, as it usually does, an inside-out patch is formed. In the inside-out patch configuration the inside of the patch of membrane is accessible and exposed to the bath (see Fig. 13.12). Alternatively, after forming a gigaohm seal, negative pressure (suction) can be applied to the inside of the patch electrode; the membrane will rupture to give electrical (and physical) access to the inside of the cell. Currents can be monitored at constant voltage from the whole cell (see Fig. 13.12). Whole cell recording can be used to monitor the activity of macroscopic currents (or in current clamp, to monitor changes in voltage) and it is currently the most commonly used configuration of the patch-clamp recording method. Finally, from the whole-cell configuration, withdrawing the patch electrode can often result in the formation of an isolated outside-out patch. In this configuration, the outside of the patch of membrane faces the bath and solutions such as agonists can be applied to activate and measure single ligand-gated ion channel currents (*Hamill et al., 1981*).

However, whole-cell recording has important limitations discussed in depth (Fenwick et al., 1982a) including:

- The loss of critical ions and molecules from the cell that may be required to maintain normal ion channel activity during the diffusional exchange between the recording electrode and the cell.
- Imperfect voltage control is often overlooked in whole-cell recording because, unlike two-microelectrode voltage-clamp, there is no independent measure of membrane voltage. In patch clamp recording the inside of the patch pipette is under voltage control and the cell membrane is clamped at the same voltage only if the resistance between the pipette and the inside of the cell is within acceptable limits. The membrane voltage of a cell can only be reliably controlled if several conditions are met: the cell is small, the electrode access resistance is sufficiently low; and the maximum currents are sufficiently small

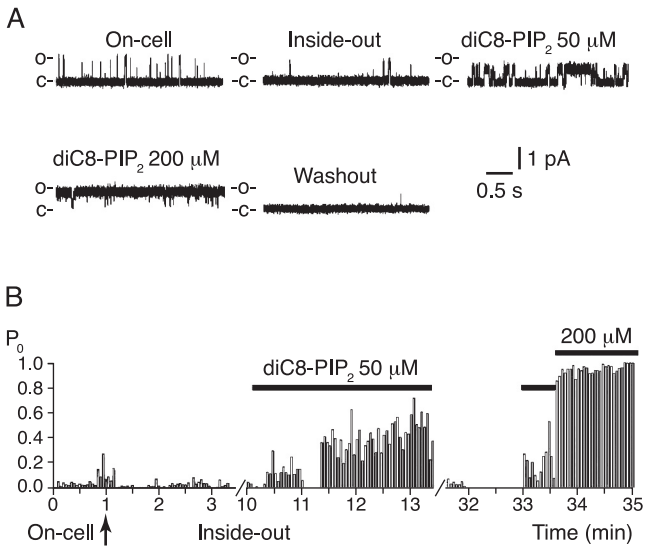

FIGURE 13.13 $K_V7.2/7.3$ single channels are activated by the water-soluble analog of PIP_2 dioctanoyl (diC8)-PIP_2. K_V currents were measured in cell-attached and inside-out patches formed from Chinese hamster ovary (CHO) cells transiently expressing $K_V7.2/7.3$ cDNAs. **A**, Outward $K_V7.2/7.3$ channel currents were observed in cell-attached patches. Channel activity decreased when the patch was excised to form an inside-out patch (see Fig. 13.16). Increasing concentrations of (diC8)-PIP_2 added to the bath (to the inside of the patch) lead to a dose-dependent increase in channel activity. **B**, The channel open probability (P_{open}) for each 3-s sweep is plotted. It shows that P_{open} increases when diC8-PIP_2 is added to the inside of the membrane patch (black bars). *Adapted from Li et al. (2005) with permission from the Society for Neuroscience.*

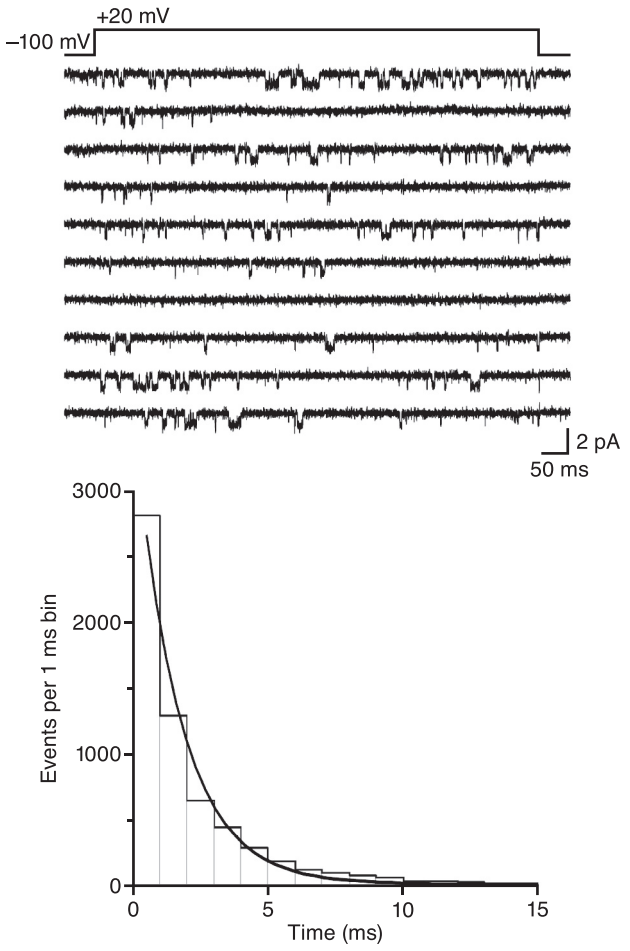

FIGURE 13.14 Single $Ca_V2.2$ channel currents recorded in a cell-attached patch show activity consistent with a single open state. Single channel currents were recorded with 110 mM Ba^{2+} in the patch pipette from tsA201 cells stably expressing $Ca_V2.2$ cDNA together with auxiliary subunits. A series of 10 consecutive single channel current sweeps are shown. Single channel currents were evoked by voltage steps to +20 mV, from a holding potential of −100 mV. The lower panel shows the open-time distribution (1-ms bin widths) of all recordings from the same patch. Open-time distributions were fit with one exponential. The time constants of open-time distribution (τ open) was 1.5 ms. *Figure adapted from Castiglioni et al. (2006).*

(Fenwick et al., 1982b). Most patch clamp amplifiers include series resistance compensation controls, but they are only effective over a limited range of values.

SINGLE ION CHANNEL CURRENTS

Single channel currents are the elementary building blocks of macroscopic whole cell currents, nicely illustrated from the ensemble averages of 80 individual single Ca_V channel sweeps (Fig. 13.11). Single channel currents provide a real time viewing of single molecules as they transition back and forth between conducting and nonconducting states.

Analyses of single channel currents provide detailed mechanistic information that can be difficult to access from macroscopic currents. The precise moment of an ion channel sojourn is not predictable—but the average behavior of a homogeneous population of channels is predictable for a defined recording condition. For example, the simplest kinetic model to describe ion channel gating has two states, closed and open:

$$C \underset{\alpha}{\overset{\beta}{\rightleftharpoons}} O \qquad (13.17)$$

The open time is exponentially distributed with a mean of $1/\alpha$ (s) (see Fig. 13.14), the reciprocal of the closing rate, and the closed time is exponentially distributed with a mean of $1/\beta$ (s), the reciprocal of the opening rate. The steady state channel open probability is the total time the channel is open divided by the total time (in closed and open states). A series of single

Ca_V channel recordings is shown in Fig. 13.14 (Castiglioni et al., 2006). The distribution of open times is fit with a single exponential consistent with a single open state and a characteristic time constant of 1.5 ms.

However VGICs, and indeed all ion channels, exist in multiple different conformational and kinetically distinct states. As discussed above for Na_V and K_V channels, VGICs have four activation particles (gates) that are voltage dependent and considered equivalent in the model shown in Fig. 13.9. VGICs are thus often represented with four closed states with 0, 1, 2 and 3 activation gates in the permissible position for channel opening, and a single open state when all four activation gates move to the permissive position (Fig. 13.9). Activation is voltage-dependent but not all steps toward channel opening have to be voltage dependent; indeed, the last transition from C to O is often best modeled as voltage-independent. VGICs also inactivate with depolarization. In these states, the channel cannot open regardless of the voltage. As illustrated in Fig. 13.8C, VGICs can inactivate from closed states as well as from the open state (see also Fig. 13.9).

Single Channel Conductance

The single channel current amplitude (i) and single channel conductance (γ) provide information about the rate of ion flow through the pore of the channel. The reversal potential gives information about the degree of ion selectivity. VGICs have highly, although not perfectly, selective ion pores such that E_{rev} tends to be close to the equilibrium potential of the ion that it conducts (E_{ion}). The theoretical equilibrium potentials for Na^+, K^+ and Ca^{2+} are approximately $+60$ mV, -90 mV, and $+123$ mV for typical mammalian cell calculated using the Nernst equation. Single channel current amplitudes of Na_V and Ca_V channels decrease as the membrane potential is depolarized, and as the driving force is reduced. This property means that as the channel open probability of Na_V and Ca_V channels increases (higher P_{open}), it becomes harder to resolve single channel events above background noise because their individual amplitudes decrease. Single K_V channel currents, by contrast, increase with membrane potential depolarization because the driving force on K^+ ions increases, and spend more time in the open state (higher P_{open}). Single Na_V and Ca_V channel currents can occasionally be captured at negative potentials when the driving force is large, but when they spend much less time open (low P_{open}). Examples of single Ca_V channel tail currents are shown in Figs. 13.10 and 13.11. In sweeps 1 and 3 in Fig. 13.10, the Ca_V channel remains open for a short time the instant the voltage step terminates and the membrane potential returns to -70 mV. Tail currents are about twice are large as the currents during test depolarization to -30 mV. The large single channel current amplitudes result from the sudden increase in the driving force at -70 mV in Fig. 13.10 and at -40 mV in Fig. 13.11, and these are the elementary currents that give rise to the tail currents in macroscopic whole cell recording shown in Fig. 13.8B.

The single channel conductance, the ease with which ions flow through the open ion pore, depends on the intrinsic properties and geometry of the ion pore, as well as the type and concentration of the permeant ions available to flow through the pore. A simple and often used procedure to increase the single channel current amplitude for improved resolution is to increase the concentration of the permeant ion. The recordings of single Ca_V channels shown in Figs. 13.10, 13.11 and Fig. 13.14 were obtained using high concentrations of Ba^{2+} as the charge carrier inside the patch pipette. Ba^{2+} flow through the pore of Ca_V1 and Ca_V2 channels meets less resistance than Ca^{2+}. Ba^{2+} also inhibits several K_V channels that, if present in the patch of membrane, could obscure Ca_V channel currents. The higher flow rates of Ba^{2+} through Ca_V1 channels are

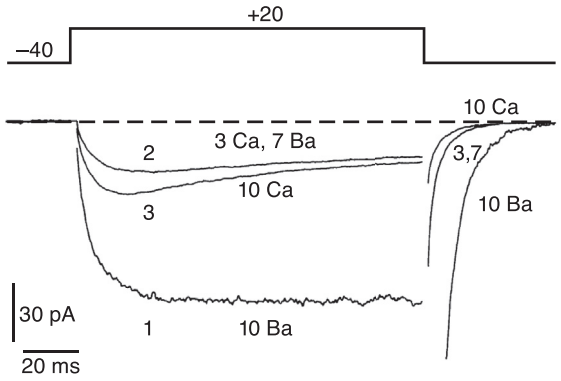

FIGURE 13.15 The anomalous mole fraction effect observed at the whole-cell level in recordings of macroscopic Ca_V1 channel currents from PC12 cells. Whole cell calcium currents were recorded using different concentration ratios of permeant ions, Ca^{2+} and Ba^{2+}. The largest peak Ca_V currents are observed when 10 mM Ba^{2+} is the charge carrier, whereas peak current amplitudes are significantly smaller with 10 mM Ca^{2+}. This is because the movement of Ca^{2+} through the Ca_V channel is impeded relative to Ba^{2+}. Peak currents measured with 7 mM Ba^{2+} and 3 mM Ca^{2+} illustrate the anomalous mole fraction effect; currents recorded under these conditions are even smaller than currents with 10 mM Ca^{2+}. Thus, peak current amplitudes change nonmonotonically as the proportion of Ba^{2+} in the solution is increased relative to Ca^{2+}. Another feature shown in this figure is Ca^{2+}-dependent inactivation which is observed as a decline in current amplitude during the test depolarization in recording with Ca^{2+} (10 Ca) but not with barium (10 Ba). Figure 13.8 illustrates the mechanism of Ca^{2+}-dependent inactivation in more detail. *Figure adapted from Friel and Tsien (1989) with permission from the authors.*

explained by the reduced interaction between Ba^{2+} and the narrow part of the Ca_V channel pore. In Ca_V1 and Ca_V2 channels, Ca^{2+} binds with μM affinity within the ion pore, preventing other cations such as Na^+ from entering. The large driving force with physiological levels of extracellular Ca^{2+} promotes inward flow of Ca^{2+} (see Fig. 13.8). Figure 13.15 illustrates the remarkable property of Ca_V1 channels to select for Ca^{2+} over other cations at the whole cell level, as well as the elegant experiments performed to demonstrate it. Macroscopic Ca_V currents recorded with 10 mM Ba^{2+} are ~three-fold larger compared to Ca^{2+} currents at equal extracellular concentrations, but currents carried by a mixture of Ca^{2+} and Ba^{2+} (maintaining the same total concentration of divalent cation) are smaller than with equi-molar concentrations of either one alone (Friel and Tsien, 1989; Hess and Tsien, 1984). Ca^{2+} inhibits the flow of Ba^{2+} through the Ca_V channel, but in the complete absence of Ca^{2+}, the Ca_V channel is highly permeable to Ba^{2+} as well as other cations.

MODULATION OF BIOPHYSICAL PROPERTIES OF VOLTAGE-GATED ION CHANNELS

The response of many VGICs to membrane depolarization is strongly influenced by a number of cellular factors including association with other proteins, second messengers, and ions. Recordings of ion currents across neuronal cell membranes reveal extraordinary diversity in their response to changes in membrane voltage even within the same family of VGICs. The diversity in time-dependent and voltage-dependent properties within the major classes of VGICs originate from the influence of cellular factors including alterative pre-mRNA splicing, association with different modulatory auxiliary subunits, chemical modifications, and binding with cytoskeletal or trafficking proteins. In this section we show how protein-protein interactions, second messenger action, and ions can affect the biophysical properties of VGICs.

Auxiliary Proteins

Auxiliary (also referred to as accessory or ancillary) subunits are proteins that associate with the central ion pore-forming α subunit of VGICs. Plasma membrane targeting of many VGICs require auxiliary proteins for trafficking from the endoplasmic reticulum. But the same auxiliary subunits may also modulate the biophysical properties of VGICs at the plasma membrane. Auxiliary subunits can be transmembrane or cytoplasmic, and they interact with different domains of α subunits. Auxiliary subunits that form relatively stable interactions with their α subunit partners are typically identified by proteomic analyses: for example, immunoprecipitation followed by Western analyses, and mass spectrometry, combined with UV-induced protein cross-linking for interactions that are disrupted by purification steps. The various auxiliary subunits that interact with and modulate the activity of K_V, Ca_V, and Na_V channels share many features including binding-partner specificity. Many auxiliary subunits modulate the gating properties of VGICs including channel activation, deactivation, inactivation, and recovery from inactivation. Less commonly, auxiliary subunits influence the rate of ion flow through open channels and single channel conductance.

Voltage-Gated Potassium Channels

K_V channels exist as multiprotein complexes at the plasma membrane, in association with four major families of auxiliary subunits: K_Vβs, KChIPs, KCNEs, and DPPLs. Each family has multiple members, and each auxiliary protein associates with specific α subunit binding partners. K_Vβs and KChIPs have conserved C-termini but variable N-termini that are proposed to determine the specificity of auxiliary protein-α subunit interaction. K_Vβ subunits modulate K_V1 channels; KChIPs modulate K_V4 channels; KCNEs and DPPLs modulate K_V7 channels.

K_Vβs can Induce N-type Inactivation of K_V1s

There are currently five members of the auxiliary K_Vβ subunit family: K_Vβ1.1, K_Vβ1.2, K_Vβ1.3, K_Vβ2, and K_Vβ3; they have unique expression patterns, and they affect the expression, activation, inactivation and deactivation of K_V1 channels. Only certain K_Vβ-K_V1 interactions are permissible.

N-type inactivation, a property of many K_V1 channels, is one of the best-understood mechanisms that result in VGIC inactivation. The N-terminal domain of K_V1 forms a physical "ball-and-chain" structure that moves into the inner mouth of the central ion pore to prevent ion flow (Armstrong, 2006) (Fig. 13.9). N-type inactivation is rapid, within 10–15 ms, and it underlies the rapid inactivation characteristic of $K_V1.4$ channels. Certain K_V1 proteins including $K_V1.1$ lack the N-terminal amino acids that form the ball and chain and, consequently, lack rapid N-type inactivation. Interestingly, some auxiliary K_Vβ subunits can mimic N-type inactivation; K_Vβ1.1 can form a ball-and-chain structure that causes rapid inactivation of K_V1 channels that lack N-type inactivation. K_Vβ1 and K_Vβ3

subunits contain ball-and-chain N-termini, but $K_V\beta2$ does not. This is physiologically important. $K_V1.1$ channels are expressed at high levels in axon membranes, including those adjacent to nerve terminals. $K_V1.1$ channels can associate with both $K_V\beta1.1$ and $K_V\beta2$. When $K_V1.1$ binds to $K_V\beta2$, it lacks N-type inactivation and has properties characteristic of a delayed-rectifier current. Therefore, the cellular expression pattern of $K_V\beta$ subunits determines the functional identity of $K_V1.1$ currents as either rapidly inactivating or noninactivating and, consequently, the firing rate of the cell. K_V4 ion channels in association with K^+ channel interacting protein (KChIP) subunits form many of the rapidly inactivating neuronal A-type K^+ currents (I_{SA}) and the cardiac transient outward current (I_{to}) (An et al., 2000; Rosati et al., 2001; Nadal et al., 2001). KChIPs associate with K_V4 channels, all four KChIP genes are expressed in brain, and one, KChIP2, is expressed in heart. KChIPs influence K_V4 expression, trafficking, activation and inactivation.

In heart, $K_V4.3$ channels underlie transient outward current (I_{to}). I_{to} currents generate the first repolarizing phase of the cardiac action potential and they are critical for normal heart function. I_{to} current amplitudes follow a gradient of increasing size from endocardium (innermost tissue) to nine-fold greater in epicardium (outermost tissue) of the ventricular free wall. The gradient of $K_V4.3$ current amplitudes is likely determined by levels of auxiliary subunit KChIP2, which also accelerate $K_V4.3$ channel recovery from inactivation (Rosati et al., 2001).

KCNE auxiliary proteins KCNE1 through KCNE5 modulate K_V7 channels (Wrobel et al., 2012; Wu et al., 2010; Kaczmarek and Blumenthal, 1997). Best studied are KCNE-$K_V7.1$ complexes in heart and cochlea. Hundreds of mutations in human $K_V7.1$ genes are linked to cardiac arrhythmias and deafness, and mutations in KCNE genes are linked to multiple human disorders. KCNE1-$K_V7.1$ channels in heart underlie slow, delayed rectifier current, I_{Ks}, which is crucial for the final repolarization phase of the cardiac action potential. KCNE1 increases surface expression of $K_V7.1$, increases single-channel conductance, and slows channel activation by shifting the voltage-dependence of channel activation to more depolarized values. The delay of $K_V7.1$ channel activation relative to Na_V is essential for the initial upstroke of the cardiac action potential.

Voltage-Gated Sodium Channels

Na_V channels associate with four auxiliary $Na_V\beta$ subunits, $Na_V\beta1$–$Na_V\beta4$ (Isom, 2001). Each Na_V protein associates with two $Na_V\beta$ subunits: one covalently bound, $Na_V\beta2$ or $Na_V\beta4$, and one noncovalently bound, $Na_V\beta1$ or $Na_V\beta3$. $Na_V\beta$ subunits are multifunctional; in addition to acting as modulators of Na_V biophysical properties, $Na_V\beta$ subunits are members of the Ig superfamily of cell adhesion molecules and regulate cell-cell adhesion and neurite outgrowth. Cerebellar granule neurons (CGNs) receive input from mossy fibers and send output to Purkinje cells via their parallel fibers. CGNs fire action potentials at rates as high as 1 kHz (1000 action potentials per second), a property that is central to rapid integration of sensory input, and rapid output of appropriate motor commands by the cerebellum. The $Na_V\beta1$ subunit is critical for normal cerebellar function. Mice lacking functional $Na_V\beta1$ proteins have severe behavioral deficits including ataxia, and reduced resurgent Na_V current that is thought to reduce the ability of CGNs to sustain high-frequency action potential firing (Brackenbury et al., 2013).

Voltage-Gated Calcium Channels

Ca_V1 and Ca_V2 channels associate with several different auxiliary subunits including $Ca_V\beta1$ through $Ca_V\beta4$ and $Ca_V\alpha_2\delta1$ through $Ca_V\alpha_2\delta4$. $Ca_V\beta1$, $\beta2b$, $\beta3$, and $\beta4$ are cytosolic proteins, while the $\beta2a$ splice isoform is palmitoylated and membrane-anchored (Dolphin, 2009). The primary binding site of $Ca_V\beta$ subunits to Ca_V1 and Ca_V2 α subunits involves a conserved motif in I-II intracellular loops (the α-interacting domain, AID) (Pragnell et al., 1994). Secondary sites of $Ca_V\beta$ binding to $Ca_V\alpha$ subunits have also been identified. $Ca_V\alpha_2\delta1$–$Ca_V\alpha_2\delta4$ subunits are known to associate with neuronal Ca_V2 channels, the α_2 and δ subunits are extracellular, disulphide-linked to each other, and δ is anchored to the plasma membrane by glycosylphosphatidylinositol (GPI) (Dolphin, 2012). $Ca_V\beta$ and $Ca_V\alpha_2\delta$ promote trafficking of Ca_V1 and Ca_V2 channels to the plasma membrane, and $Ca_V\beta$ contains a motif that occludes endoplasmic reticulum (ER) retention motif in Ca_V1 and Ca_V2 channels and displaces them from the ER. $Ca_V\beta$ and $Ca_V\alpha_2\delta$ also modulate the biophysical properties of certain Ca_V channels including the kinetics of activation, inactivation, and deactivation, as well as sensitivity to other ion channel modulators such as G proteins and calcium. $Ca_V\beta1b$, $Ca_V\beta2a$, $Ca_V\beta3$ and $Ca_V\beta4$ subunits have unique actions on cardiac $Ca_V1.2$ channels. For example, $Ca_V\beta1b$ decreases whereas $Ca_V\beta2a$ increases single $Ca_V1.2$ channel P_{open}, and $Ca_V\beta2a$ slows $Ca_V1.2$ channel closing relative to $Ca_V\beta1b$ or $Ca_V\beta3$ subunits. The effect of different $Ca_V\beta2$ subunits on the gating of single $Ca_V1.2$ channels is shown in Fig. 13.16 (Colecraft et al., 2002).

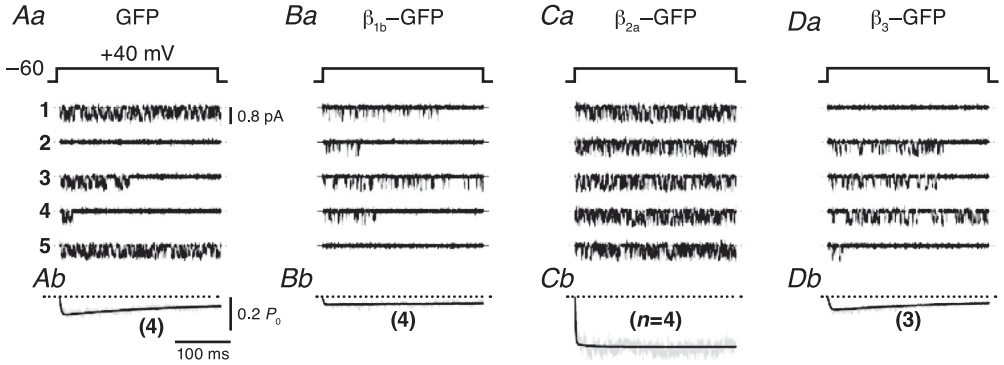

FIGURE 13.16 The effects of different $Ca_V\beta$ subunits on the gating properties of single Ca_V1 channels. Single channel Ca_V1 currents were recorded in cell attached patches from heart cells using 90 mM Ba^{2+} as the charge carrier inside the patch pipette. Different $Ca_V\beta$ subunits were overexpressed in heart cells and visualized with a GFP tag. Control cells were transfected with the GFP tag alone (Aa). Single Ca_V channel currents were activated by voltage steps to +40 mV from a holding potential of −60 mV. Currents were recorded from cells expressing β_{1b}, β_{2a} and β_3 subunits. Ensemble currents from averaging a large number of individual sweeps at the same potential are shown below each condition. The β_{2a} subunit increases the single channel P_{open}, increases the overall size of the current, and appears to remove inactivation relative to recordings from control cells as well as from those expressing β_{1b} or β_{2a}. *Figure adapted from Colecraft et al. (2002) with permission. Copyright 2004, John Wiley and Sons Ltd.*

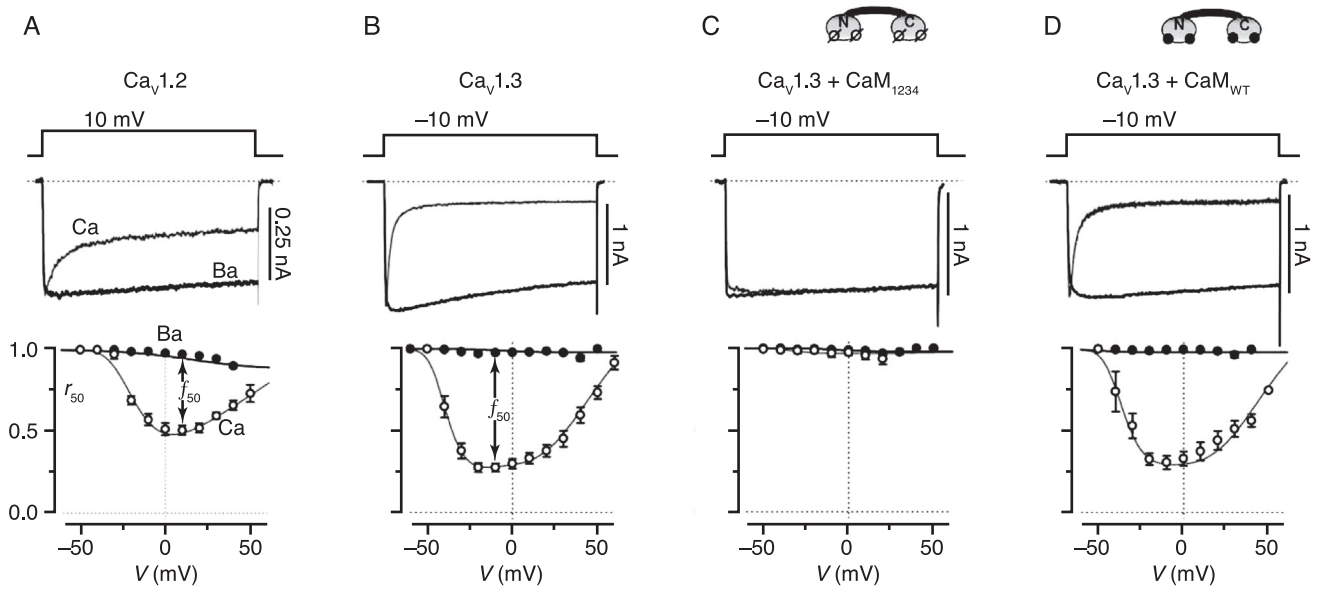

FIGURE 13.17 Whole cell $Ca_V1.2$ and $Ca_V1.3$ currents show strong calcium-dependent inactivation that depends on the presence of wild-type calmodulin. Whole cell $Ca_V1.2$ and $Ca_V1.3$ currents were recorded from tsA201 cells expressing $Ca_V1.2$ and $Ca_V1.3$ cDNAs together with the necessary auxiliary subunits, with or without calmodulin. $Ca_V1.3$ currents show very strong calcium-dependent inactivation (CDI) and this depends exclusively on the presence of wild-type calmodulin (CaM). The darker current recordings were obtained using Ba^{2+} as the charge carrier (CDI absent), whereas the lighter currents were recorded with Ca^{2+} as the charge carrier (CDI present). The fraction of peak current remaining after a 50-ms depolarization (r50) is plotted against the test potential for recordings obtained with Ba^{2+} and Ca^{2+} as the charge carriers, and shown below each condition. The step depolarizations are 300 ms long. **A**, CDI exhibited by $Ca_V1.2$ channels ($n = 6$ for IV plots). **B**, very strong CDI exhibited by $Ca_V1.3$ channels ($n = 11$ for IV plots), **C**, CDI is abolished in $Ca_V1.3$ channels when the mutant form of CaM, CaM_{1234} is expressed. CaM_{1234} was rendered Ca^{2+} insensitive by mutating all four EF-hand Ca^{2+} binding sites ($n = 7$ for IV plots). **D**, no additional CDI observed in $Ca_V1.3$ channels when wild-type CaM is overexpressed ($n = 5$ for IV plots). *Adapted from Yang et al. (2006) with permission from the Society for Neuroscience.*

LOCAL CHANGES IN CHEMICAL ENVIRONMENT BY SECOND MESSENGER ACTION

VGICs are the targets of many second messengers that result in transient changes in neuronal excitability. Second messengers regulate the activity of many protein kinases and phosphatases that control the phosphorylation state of strategically located threonine, serine, and tyrosine amino acids in VGICs.

Phosphorylation of $K_V3.1$ Promotes High-Frequency Action Potential Firing

In the central auditory system, neurons that encode high-frequency sound waves must reproduce those stimuli via high rates of action potential firing with absolute temporal precision (up to ~800 Hz). The presynaptic bouton of the Calyx of Held synapse (from a neuron in the ventral cochlear nucleus) is like a glove surrounding its postsynaptic partner, the cell body of a principle neuron of the medial nucleus of the trapezoid body (MNTB). Its large size permits simultaneous recordings from both pre- and postsynaptic terminals. $K_V3.1$ channels in MNTB neurons undergo very rapid voltage-dependent activation and deactivation; these channels are particularly important for the ability of MNTB neurons to fire action potentials at high rates (Macica et al., 2003). High frequency stimulation leads to rapid dephosphorylation of $K_V3.1$, facilitating current amplitudes and supporting high firing rates in MNTB neurons; low frequency stimulation leads to rapid PKA-dependent phosphorylation of serine in $K_V3.1$, facilitating decreased $K_V3.1$ activity and lower firing rates in MNTB neurons.

Phosphorylation Modulates Activity of Na_v Channels

Neuronal $Na_V1.7$ and $Na_V1.8$ channels are regulated by the activity of p38 MAPK and ERKI/II protein kinases, and $Na_V1.2$ channel activity by the growth factor BDNF. BDNF activation of its receptor TrkB activates an intermediary kinase, which in turn phosphorylates tyrosine residues on $Na_V1.2$, and this accelerates channel inactivation and promotes voltage-dependent inactivation at more hyperpolarized membrane potentials.

The cardiac $Na_V1.5$ channel is regulated by the calcium/calmodulin kinase II (CaMKII). CaMKII attenuates Na_V channel function by promoting steady-state inactivation, and factors that inhibit CaMKII prolong action potentials in heart. Several protein kinases including Protein Kinase A (PKA) and Protein Kinase C (PKC) target amino acids serine, threonine and tyrosine in neuronal $Na_V1.1$, $Na_V1.2$ and cardiac $Na_V1.5$ channels to regulate their activity. Phosphorylation of specific threonine and serine residues in the intracellular loop between domains I and II enhance slow inactivation of Na_V channels and lead to reduced Na_V current.

Phosphorylation Modulates Activity of Ca_v Channels

One of the first and classic examples of phosphorylation-dependent regulation of VGICs, published by Reuter and colleagues, is β-adrenergic facilitation of cardiac Ca_V1 channels through cAMP and protein kinase A in the fight-or-flight response (Reuter and Porzig, 1982; Cachelin et al., 1983). Since these pioneering studies by Reuter and colleagues, numerous transmitters, drugs, and hormones have been shown to regulate Ca_V ion channel activity through various kinases and phosphatases (DeRiemer et al., 1985; Kaczmarek, 1988; Su et al., 2012; Sanderson et al., 2012; Higley and Sabatini, 2010; Bender et al., 2010; Dai et al., 2009), and the precise amino acid targets of kinase-dependent phosphorylation on Ca_V channels continue to be identified (Fu et al., 2013). In neurons, protein kinase A, protein kinase C, cyclin dependent kinase 5 (Cdk5), mitogen-activated protein kinase (MAPK), extracellular signal-regulated kinase (ERK), glycogen synthase kinase-3 (GSK-3) are implicated in either augmenting or inhibiting Ca_V channel function. Similarly, protein phosphatases, calcineurin (Evans et al., 2013; Oliveria et al., 2012) and PP2A (Dai et al., 2009), act on Ca_V channels and modulate their activities. Kinase and phosphatase actions on Ca_V channels are spatially and temporally restricted within signaling complexes; these include scaffolding proteins and regulators of kinase and phosphatase action depending on cell-type and subcellular location (Dai et al., 2009).

NEUROTOXINS THAT DISRUPT BIOPHYSICAL PROPERTIES OF VGICS

Ion channel neurotoxins can be divided into two major categories: hydrophilic peptides that recognize extracellular binding sites on channels, and lipid-permeable toxins that can cross the plasma membrane and access intracellular targets (Table 13.2). Neurotoxins have been isolated from a wide variety of animals and plants, including spiders, snakes, bacteria, and scorpions (Table 13.2). Many of these toxins share remarkable sequence similarity, and many have the

same protein target. Ca_V and Na_V channels are excellent targets of venomous species because of their critical roles in neurotransmission. Many neurotoxins act by either inhibiting or augmenting ion channel activity, and most lethal venoms contain a spectrum of neurotoxins with actions on multiple essential ion channels and receptors at synapses. Toxins that act on Na_V channels have offered invaluable insight into the biophysical properties of Na_V channels and the structural domains that regulate them (Fig. 13.1B). For example, the pufferfish neurotoxin tetrodotoxin (TTX) binds and occludes the extracellular mouth of the ion pore of many Na_V channels. This toxin–channel interaction was used to identify amino acids present in the outer mouth of the Na_V channel prior to crystal structure determination.

Na_V neurotoxins come in six varieties based on the region of Na_V that they bind: 1–6 (see Fig. 13.1B and Table 13.2). Their binding locations tend to be predictive of their biophysical actions on Na_V function. For example, α-toxins from scorpions and sea anemones bind to site 3 of Na_V channels and slow inactivation and β-toxins from other scorpions and spiders bind to site 4 of Na_V channels and promote voltage-dependent activation.

Some neurotoxins are described as state-dependent: they bind or stabilize Na_V channels in specific conformational states. For example, the binding and action of α-toxins is weakened at depolarized voltages that promote inactivation, suggesting that α-toxins bind preferentially to closed or open, but not inactivated channels; α-toxins slow transitions of Na_V channels into inactivated states, resulting in larger Na_V currents and prolonged action potentials.

Membrane-permeable Na_V toxins include grayanotoxins from plants of the heather family and batrachotoxins isolated from Colombian poison dart frogs. Grayanotoxins and batrachotoxins bind to site 2 on the transmembrane segment 6 of Na_V. Their actions are state-dependent but, different from α-toxins, grayanotoxin and batrachotoxin only bind to, or dissociate from, open Na_V channels. These toxins influence Na_V channel gating and ion permeation; they promote voltage-dependent activation and slow or eliminate inactivation, and the ion pore loses Na^+ selectively and becomes permeable to potassium ions.

THE PLASMA MEMBRANE LIPID PIP_2 MODULATES VGICS

Phosphatidylinositol 4,5-bisphosphate (PIP_2) is a minor phospholipid found only in the plasma membrane inner leaflet and it plays an important role in modulating VGIC activity. PIP_2 is reported to influence the activity of over 80 different ion channels including $K_V1.1$, $K_V1.2$, $K_V1.4$, $K_V3.4$, $Ca_V1.3$, $Ca_V2.1$ and $Ca_V2.2$. However, its effects are complex and may depend on several factors including the cellular environment. Research on the actions of PIP_2 is ongoing, but there is general agreement that it is a critical cellular regulator of many VGICs.

Inhibitory Effects of PIP_2

The headgroup of PIP_2 carries a net negative charge, the S4–S5 linker of VGICs carries a net positive charge, and the two are thought to interact. The S4–S5 linker is central to coupling the VSD to the PD in VGICs and the binding of PIP_2. It has been shown that PIP_2 can stabilize or constrain the movement of S4, decreasing the coupling efficiency between voltage-sensing and channel pore opening of $K_V1.2$, thereby favoring the closed state. This form of inhibition of $K_V1.2$ channels by PIP_2 is voltage-dependent.

G protein coupled receptors that signal through $G\alpha_q$ subunits (GqPCRs) activate phospholipase C (PLC) which hydrolyzes PIP_2 into IP_3 and DAG (note: these are signaling molecules with their own specific activity). GqPCRs including M1 muscarinic acetylcholine receptor (M1R) inhibit certain Ca_V and K_V channels by a mechanism attributed to depletion of membrane PIP_2. Depletion of PIP_2 left-shifts the voltage-dependence of activation but also decreases channel open probability, leading overall to a decrease in current amplitude. Thus certain VGICs including Ca_V1, Ca_V2, and $K_V1.2$ require the presence of PIP_2 to be available for activation; in the absence of PIP_2 channel activity is labile (see Fig. 13.13).

CALCIUM INACTIVATES Ca_V1 CHANNELS

A characteristic feature of Ca_V1 channels is calcium-dependent inactivation (CDI). CDI is an autoregulatory mechanism in which the Ca^{2+} ions that flow through the ion pore of Ca_V channels also inactivate the channel during sustained depolarization. CDI is mediated by calmodulin (CaM), which is prebound to the C-terminus of Ca_V1 channels in the absence of Ca^{2+}, and rapidly mediates Ca_V channel inactivation when fully occupied by four Ca^{2+} ions. Mutant, inactive forms of CaM (e.g. CaM1234) do not support CDI of Ca_V1 channels (Fig. 13.17) (Yang et al., 2006; Dick et al., 2008).

$Ca_V1.3$ channels expressed in heart and neurons exhibit CDI but those in the inner ear and in $Ca_V1.4$ channels in photoreceptors have very little CDI. The

lack of CDI seen in Ca_V1 channels of inner ear and photoreceptors is physiologically significant because constant Ca^{2+} influx is needed in these cells during prolonged depolarization, to support tonic release of transmitter. What factors control CDI in $Ca_V1.3$ and $Ca_V1.4$ channels expressed in different cells? Full-length $Ca_V1.3$ and $Ca_V1.4$ channels contain distal C-terminal autoinhibitory domains that occlude the binding of CaM, preventing CDI. Different cells express different splice isoforms of $Ca_V1.3$ channels with different C-termini, and thus with different degrees of CDI (Dick et al., 2008). In addition, certain proteins such as CaBP4 are expressed in hair cells and interfere with CaM binding and CDI of $Ca_V1.3$ channels (Cui et al., 2007).

$Ca_V1.3$ channels in outer hair cells of the ear also exhibit little CDI, because the particular splice isoform of $Ca_V1.3$ ($Ca_V1.3[\Delta41]$) expressed in these cells lacks the domain that binds CaM in other forms of $Ca_V1.3$. Point mutations in the human $Ca_V1.4$ gene (*Cacna1f*) that truncate $Ca_V1.4$ are thought to cause congenital stationary night blindness (CSNB) (Table 13.1). Truncated $Ca_V1.4$ channels lack an autoinhibitory module that would otherwise interfere with CaM binding in the proximal region of the C-terminus of $Ca_V1.4$. In expression systems, truncated $Ca_V1.4$ channels have robust CDI (Wahl-Schott et al., 2006).

We like to define proteins including ion channels according to specific functional properties. As discussed at the start of this chapter, certain features of VGICs such as ion selectivity are static and critical for functional integrity. By contrast, the voltage-dependent and time-dependent characteristics of VGIC activation, deactivation, inactivation and recovery from inactivation vary among VGIC families, are dynamic, and are influenced by a range of cellular factors. Elegant cellular mechanisms have evolved to regulate these biophysical properties of VGICs including alternative pre-mRNA splicing, cell-specific protein–protein interactions, kinase-dependent phosphorylation of critical serine, threonine or tyrosine amino acids, G protein coupled receptor-dependent changes in membrane phospholipid PIP_2 and other second messengers, and auto-inhibitory feedback that utilizes the conducting ion. Toxins have also evolved that target the specific structures of VGICs that control their activity. Cellular and natural regulators of VGICs reveal critical domains on channels that control their activity and help us understand the significance of VGICs in cell function.

Acknowledgements

We are grateful to Dr. Arturo Andrade for providing recordings of Ca_V channel currents shown in Fig. 13.8, and to Erin Hoops for the simulations of Na_V and K_V currents shown in Fig. 13.7.

References

Ahern, C.A., Horn, R., 2005. Focused electric field across the voltage sensor of potassium channels. Neuron. 48, 25–29.

Almers, W., McCleskey, E.W., 1984. Non-selective conductance in calcium channels of frog muscle: calcium selectivity in a single-file pore. J. Physiol. 353, 585–608.

An, W.F., Bowlby, M.R., Betty, M., Cao, J., Ling, H.P., Mendoza, G., et al., 2000. Modulation of A-type potassium channels by a family of calcium sensors. Nature. 403, 553–556.

Armstrong, C.M., 2006. Na channel inactivation from open and closed states. Proc. Natl. Acad. Sci. USA. 103, 17991–17996.

Armstrong, C.M., Bezanilla, F., 1974. Charge movement associated with the opening and closing of the activation gates of the Na channels. J. Gen. Physiol. 63, 533–552.

Bech-Hansen, N.T., Naylor, M.J., Maybaum, T.A., Pearce, W.G., Koop, B., Fishman, G.A., et al., 1998. Loss-of-function mutations in a calcium-channel alpha1-subunit gene in Xp11.23 cause incomplete X-linked congenital stationary night blindness. Nat. Genet. 19, 264–267.

Bender, K.J., Ford, C.P., Trussell, L.O., 2010. Dopaminergic modulation of axon initial segment calcium channels regulates action potential initiation. Neuron. 68, 500–511.

Bezanilla, F., 2008. Ion channels: from conductance to structure. Neuron. 60, 456–468.

Brackenbury, W.J., Yuan, Y., O'Malley, H.A., Parent, J.M., Isom, L.L., 2013. Abnormal neuronal patterning occurs during early postnatal brain development of Scn1b-null mice and precedes hyperexcitability. Proc. Natl. Acad. Sci. USA. 110, 1089–1094.

Cachelin, A.B., de Peyer, J.E., Kokubun, S., Reuter, H., 1983. Ca^{2+} channel modulation by 8-bromocyclic AMP in cultured heart cells. Nature. 304, 462–464.

Castaneda, O., Harvey, A.L., 2009. Discovery and characterization of cnidarian peptide toxins that affect neuronal potassium ion channels. Toxicon. 54, 1119–1124.

Castiglioni, A.J., Raingo, J., Lipscombe, D., 2006. Alternative splicing in the C-terminus of $Ca_V2.2$ controls expression and gating of N-type calcium channels. J. Physiol. 576, 119–134.

Catterall, W.A., 2011. Voltage-gated calcium channels. Cold Spring Harb. Perspect. Biol. 3, a003947.

Catterall, W.A., Leal, K., Nanou, E., 2013. Calcium channels and short-term synaptic plasticity. J. Biol. Chem. 288, 10742–10749.

Chen, J., Mitcheson, J.S., Tristani-Firouzi, M., Lin, M., Sanguinetti, M. C., 2001. The S4-S5 linker couples voltage sensing and activation of pacemaker channels. Proc. Natl. Acad. Sci. USA. 98, 11277–11282.

Colecraft, H.M., Alseikhan, B., Takahashi, S.X., Chaudhuri, D., Mittman, S., Yegnasubramanian, V., et al., 2002. Novel functional properties of Ca^{2+} channel beta subunits revealed by their expression in adult rat heart cells. J. Physiol. 541, 435–452.

Crandall, S.R., Govindaiah, G., Cox, C.L., 2010. Low-threshold Ca^{2+} current amplifies distal dendritic signaling in thalamic reticular neurons. J. Neurosci. 30, 15419–15429.

Cui, G., Meyer, A.C., Calin-Jageman, I., Neef, J., Haeseleer, F., Moser, T., et al., 2007. Ca^{2+}-binding proteins tune Ca^{2+}-feedback to $Ca_V1.3$ channels in mouse auditory hair cells. J. Physiol. 585, 791–803.

Dai, S., Hall, D.D., Hell, J.W., 2009. Supramolecular assemblies and localized regulation of voltage-gated ion channels. Physiol. Rev. 89, 411–452.

DeRiemer, S.A., Strong, J.A., Albert, K.A., Greengard, P., Kaczmarek, L.K., 1985. Enhancement of calcium current in Aplysia neurones by phorbol ester and protein kinase C. Nature. 313, 313–316.

Dib-Hajj, S.D., Rush, A.M., Cummins, T.R., Hisama, F.M., Novella, S., Tyrrell, L., et al., 2005. Gain-of-function mutation in Nav1.7 in familial erythromelalgia induces bursting of sensory neurons. Brain. 128, 1847–1854.

Dick, I.E., Tadross, M.R., Liang, H., Tay, L.H., Yang, W., Yue, D.T., 2008. A modular switch for spatial Ca^{2+} selectivity in the calmodulin regulation of Ca_V channels. Nature. 451, 830–834.
Dolphin, A.C., 2009. Calcium channel diversity: multiple roles of calcium channel subunits. Curr. Opin. Neurobiol. 19, 237–244.
Dolphin, A.C., 2012. Calcium channel auxiliary alpha2delta and beta subunits: trafficking and one step beyond. Nat. Rev. Neurosci. 13, 542–555.
Doyle, D.A., Morais Cabral, J., Pfuetzner, R.A., Kuo, A., Gulbis, J.M., Cohen, S.L., et al., 1998. The structure of the potassium channel: molecular basis of K^+ conduction and selectivity. Science. 280, 69–77.
Du, X., Wang, J., Zhu, H., Rinaldo, L., Lamar, K.M., Palmenberg, A. C., et al., 2013. Second cistron in CACNA1A gene encodes a transcription factor mediating cerebellar development and SCA6. Cell. 154, 118–133.
Estacion, M., Dib-Hajj, S.D., Benke, P.J., Te Morsche, R.H., Eastman, E.M., Macala, L.J., et al., 2008. NaV1.7 gain-of-function mutations as a continuum: A1632E displays physiological changes associated with erythromelalgia and paroxysmal extreme pain disorder mutations and produces symptoms of both disorders. J. Neurosci. 28, 11079–11088.
Evans, M.D., Sammons, R.P., Lebron, S., Dumitrescu, A.S., Watkins, T.B., Uebele, V.N., et al., 2013. Calcineurin signaling mediates activity-dependent relocation of the axon initial segment. J. Neurosci. 33, 6950–6963.
Fatt, P., Ginsborg, B.L., 1958. The production of regenerative responses in crayfish muscle fibres by the action of calcium, strontium and barium. J. Physiol. 140, 59–60P.
Fenwick, E.M., Marty, A., Neher, E., 1982a. A patch-clamp study of bovine chromaffin cells and of their sensitivity to acetylcholine. J. Physiol. 331, 577–597.
Fenwick, E.M., Marty, A., Neher, E., 1982b. Sodium and calcium channels in bovine chromaffin cells. J. Physiol. 331, 599–635.
Fertleman, C.R., Baker, M.D., Parker, K.A., Moffatt, S., Elmslie, F.V., Abrahamsen, B., et al., 2006. SCN9A mutations in paroxysmal extreme pain disorder: allelic variants underlie distinct channel defects and phenotypes. Neuron. 52, 767–774.
Friel, D.D., Tsien, R.W., 1989. Voltage-gated calcium channels: direct observation of the anomalous mole fraction effect at the single-channel level. Proc. Natl. Acad. Sci. USA. 86, 5207–5211.
Fu, Y., Westenbroek, R.E., Scheuer, T., Catterall, W.A., 2013. Phosphorylation sites required for regulation of cardiac calcium channels in the fight-or-flight response. Proc. Natl. Acad. Sci. USA..
Hagiwara, S., Byerly, L., 1981. Calcium channel. Annu. Rev. Neurosci. 4, 69–125.
Hamill, O.P., Marty, A., Neher, E., Sakmann, B., Sigworth, F.J., 1981. Improved patch-clamp techniques for high-resolution current recording from cells and cell-free membrane patches. Pflugers. Arch. 391, 85–100.
Hegle, A.P., Marble, D.D., Wilson, G.F., 2006. A voltage-driven switch for ion-independent signaling by ether-a-go-go K^+ channels. Proc. Natl. Acad. Sci. USA. 103, 2886–2891.
Hess, P., Tsien, R.W., 1984. Mechanism of ion permeation through calcium channels. Nature. 309, 453–456.
Hess, P., Lansman, J.B., Tsien, R.W., 1986. Calcium channel selectivity for divalent and monovalent cations. Voltage and concentration dependence of single channel current in ventricular heart cells. J. Gen. Physiol. 88, 293–319.
Higley, M.J., Sabatini, B.L., 2010. Competitive regulation of synaptic Ca^{2+} influx by D2 dopamine and A2A adenosine receptors. Nat. Neurosci. 13, 958–966.
Hille, B., 2001. Ion Channels of Excitable Membranes. Sinauer, Sunderland, Mass.
Hodgkin, A.L., Huxley, A.F., 1952. A quantitative description of membrane current and its application to conduction and excitation in nerve. J. Physiol. 117, 500–544.
Horn, R., Patlak, J., 1980. Single channel currents from excised patches of muscle membrane. Proc. Natl. Acad. Sci. USA. 77, 6930–6934.
Isom, L.L., 2001. Sodium channel beta subunits: anything but auxiliary. Neuroscientist. 7, 42–54.
Johnson, S.L., Marcotti, W., 2008. Biophysical properties of $Ca_V1.3$ calcium channels in gerbil inner hair cells. J. Physiol. 586, 1029–1042.
Kaczmarek, L.K., 1988. The regulation of neuronal calcium and potassium channels by protein phosphorylation. Adv. Second Messenger Phosphoprotein Res. 22, 113–138.
Kaczmarek, L.K., Blumenthal, E.M., 1997. Properties and regulation of the minK potassium channel protein. Physiol. Rev. 77, 627–641.
Kang, S., Cooper, G., Dunne, S.F., Dusel, B., Luan, C.H., Surmeier, D.J., et al., 2012. $Ca_V1.3$-selective L-type calcium channel antagonists as potential new therapeutics for Parkinson's disease. Nat. Commun. 3, 1146.
Katz, B., 1966. Nerve, Muscle and Synapse. McGraw-Hill Inc..
Kavalali, E.T., Plummer, M.R., 1994. Selective potentiation of a novel calcium channel in rat hippocampal neurones. J. Physiol. 480, 475–484.
Knapp, O., McArthur, J.R., Adams, D.J., 2012. Conotoxins targeting neuronal voltage-gated sodium channel subtypes: potential analgesics?. Toxins (Basel). 4, 1236–1260.
Leal, K., Mochida, S., Scheuer, T., Catterall, W.A., 2012. Fine-tuning synaptic plasticity by modulation of $Ca_V2.1$ channels with Ca^{2+} sensor proteins. Proc. Natl. Acad. Sci. USA. 109, 17069–17074.
Lee, A., Wong, S.T., Gallagher, D., Li, B., Storm, D.R., Scheuer, T., et al., 1999. Ca^{2+}/calmodulin binds to and modulates P/Q-type calcium channels. Nature. 399, 155–159.
Lee, A., Zhou, H., Scheuer, T., Catterall, W.A., 2003. Molecular determinants of Ca^{2+}/calmodulin-dependent regulation of $Ca_V2.1$ channels. Proc. Natl. Acad. Sci. USA. 100, 16059–16064.
Li, Y., Gamper, N., Hilgemann, D.W., Shapiro, M.S., 2005. Regulation of K_V7 (KCNQ) K^+ channel open probability by phosphatidylinositol 4,5-bisphosphate. J. Neurosci. 25, 9825–9835.
Lin, Y., McDonough, S.I., Lipscombe, D., 2004. Alternative splicing in the voltage-sensing region of N-Type $Ca_V2.2$ channels modulates channel kinetics. J. Neurophysiol. 92, 2820–2830.
Lipscombe, D., Allen, S.E., Toro, C.P., 2013. Control of neuronal voltage-gated calcium ion channels from RNA to protein. Trends Neurosci. 36, 598–609.
Long, S.B., Campbell, E.B., Mackinnon, R., 2005. Voltage sensor of $K_V1.2$: structural basis of electromechanical coupling. Science. 309, 903–908.
Morgans, C.W., 2001. Localization of the alpha(1F) calcium channel subunit in the rat retina. Invest Ophthalmol. Vis. Sci. 42, 2414–2418.
Nadal, M.S., Amarillo, Y., Vega-Saenz de Miera, E., Rudy, B., 2001. Evidence for the presence of a novel K_V4-mediated A-type K^+ channel-modifying factor. J. Physiol. 537, 801–809.
Neher, E., Sakmann, B., 1976. Single-channel currents recorded from membrane of denervated frog muscle fibres. Nature. 260, 799–802.
Oliveria, S.F., Dittmer, P.J., Youn, D.H., Dell'Acqua, M.L., Sather, W.A., 2012. Localized calcineurin confers Ca^{2+}-dependent inactivation on neuronal L-type Ca^{2+} channels. J. Neurosci. 32, 15328–15337.
Parajuli, L.K., Nakajima, C., Kulik, A., Matsui, K., Schneider, T., Shigemoto, R., et al., 2012. Quantitative regional and ultrastructural localization of the $Ca_v2.3$ subunit of R-type calcium channel in mouse brain. J. Neurosci. 32, 13555–13567.

Payandeh, J., Scheuer, T., Zheng, N., Catterall, W.A., 2011. The crystal structure of a voltage-gated sodium channel. Nature. 475, 353–358.

Peterson, B.Z., DeMaria, C.D., Adelman, J.P., Yue, D.T., 1999. Calmodulin is the Ca^{2+} sensor for Ca^{2+} -dependent inactivation of L-type calcium channels. Neuron. 22, 549–558.

Pragnell, M., De Waard, M., Mori, Y., Tanabe, T., Snutch, T.P., Campbell, K.P., 1994. Calcium channel beta-subunit binds to a conserved motif in the I-II cytoplasmic linker of the alpha 1-subunit. Nature. 368, 67–70.

Pringos, E., Vignes, M., Martinez, J., Rolland, V., 2011. Peptide neurotoxins that affect voltage-gated calcium channels: a close-up on omega-agatoxins. Toxins (Basel). 3, 17–42.

Putzier, I., Kullmann, P.H., Horn, J.P., Levitan, E.S., 2009. $Ca_V1.3$ channel voltage dependence, not Ca^{2+} selectivity, drives pacemaker activity and amplifies bursts in nigral dopamine neurons. J. Neurosci. 29, 15414–15419.

Reuter, H., Porzig, H., 1982. Beta-adrenergic actions on cardiac cell membranes. Adv. Myocardiol. 3, 87–93.

Rios, E., Brum, G., 1987. Involvement of dihydropyridine receptors in excitation-contraction coupling in skeletal muscle. Nature. 325, 717–720.

Rodriguez-Menchaca, A.A., Adney, S.K., Tang, Q.Y., Meng, X.Y., Rosenhouse-Dantsker, A., Cui, M., et al., 2012. PIP2 controls voltage-sensor movement and pore opening of K_V channels through the S4-S5 linker. Proc. Natl. Acad. Sci. USA. 109, E2399–E2408.

Rosati, B., Pan, Z., Lypen, S., Wang, H.S., Cohen, I., Dixon, J.E., et al., 2001. Regulation of KChIP2 potassium channel beta subunit gene expression underlies the gradient of transient outward current in canine and human ventricle. J. Physiol. 533, 119–125.

Sanderson, J.L., Gorski, J.A., Gibson, E.S., Lam, P., Freund, R.K., Chick, W.S., et al., 2012. AKAP150-anchored calcineurin regulates synaptic plasticity by limiting synaptic incorporation of Ca^{2+}-permeable AMPA receptors. J. Neurosci. 32, 15036–15052.

Schjott, J.M., Plummer, M.R., 2000. Sustained activation of hippocampal Lp-type voltage-gated calcium channels by tetanic stimulation. J. Neurosci. 20, 4786–4797.

Schneider, M.F., Chandler, W.K., 1973. Voltage dependent charge movement of skeletal muscle: a possible step in excitation-contraction coupling. Nature. 242, 244–246.

Schoppa, N.E., McCormack, K., Tanouye, M.A., Sigworth, F.J., 1992. The size of gating charge in wild-type and mutant Shaker potassium channels. Science. 255, 1712–1715.

Schulte, U., Thumfart, J.O., Klocker, N., Sailer, C.A., Bildl, W., Biniossek, M., et al., 2006. The epilepsy-linked Lgi1 protein assembles into presynaptic K_V1 channels and inhibits inactivation by $K_V$beta1. Neuron. 49, 697–706.

Shtonda, B., Avery, L., 2005. CCA-1, EGL-19 and EXP-2 currents shape action potentials in the Caenorhabditis elegans pharynx. J. Exp. Biol. 208, 2177–2190.

Sigworth, F.J., 1986. The patch clamp is more useful than anyone had expected. Fed. Proc. 45, 2673–2677.

Sigworth, F.J., Neher, E., 1980. Single Na^+ channel currents observed in cultured rat muscle cells. Nature. 287, 447–449.

Sokolov, S., Scheuer, T., Catterall, W.A., 2007. Gating pore current in an inherited ion channelopathy. Nature. 446, 76–78.

Sokolov, S., Scheuer, T., Catterall, W.A., 2008. Depolarization-activated gating pore current conducted by mutant sodium channels in potassium-sensitive normokalemic periodic paralysis. Proc. Natl. Acad. Sci. USA. 105, 19980–19985.

Starace, D.M., Bezanilla, F., 2004. A proton pore in a potassium channel voltage sensor reveals a focused electric field. Nature. 427, 548–553.

Su, S.C., Seo, J., Pan, J.Q., Samuels, B.A., Rudenko, A., Ericsson, M., et al., 2012. Regulation of N-type voltage-gated calcium channels and presynaptic function by cyclin-dependent kinase 5. Neuron. 75, 675–687.

Tanabe, T., Beam, K.G., Powell, J.A., Numa, S., 1988. Restoration of excitation-contraction coupling and slow calcium current in dysgenic muscle by dihydropyridine receptor complementary DNA. Nature. 336, 134–139.

Wahl-Schott, C., Baumann, L., Cuny, H., Eckert, C., Griessmeier, K., Biel, M., 2006. Switching off calcium-dependent inactivation in L-type calcium channels by an autoinhibitory domain. Proc. Natl. Acad. Sci. USA. 103, 15657–15662.

Wheeler, D.G., Groth, R.D., Ma, H., Barrett, C.F., Owen, S.F., Safa, P., et al., 2012. Ca_V1 and Ca_V2 channels engage distinct modes of Ca^{2+} signaling to control CREB-dependent gene expression. Cell. 149, 1112–1124.

Wrobel, E., Tapken, D., Seebohm, G., 2012. The KCNE Tango – How KCNE1 Interacts with $K_V7.1$. Front Pharmacol. 3, 142.

Wu, D., Pan, H., Delaloye, K., Cui, J., 2010. KCNE1 remodels the voltage sensor of $K_V7.1$ to modulate channel function. Biophys. J. 99, 3599–3608.

Yang, J., Ellinor, P.T., Sather, W.A., Zhang, J.F., Tsien, R.W., 1993. Molecular determinants of Ca^{2+} selectivity and ion permeation in L-type Ca^{2+} channels. Nature. 366, 158–161.

Yang, P.S., Alseikhan, B.A., Hiel, H., Grant, L., Mori, M.X., Yang, W., et al., 2006. Switching of Ca^{2+}-dependent inactivation of $Ca_V1.3$ channels by calcium binding proteins of auditory hair cells. J. Neurosci. 26, 10677–10689.